Atmospheric
Chemistry
and Physics

Temporal variations of atmospheric CO_2 and CO at Ahmedabad in western India

Naveen Chandra[1,2]**, Shyam Lal**[1]**, S. Venkataramani**[1]**, Prabir K. Patra**[3]**, and Varun Sheel**[1]

[1]Physical Research Laboratory Ahmedabad 380009, India
[2]Indian Institute of Technology, Gandhinagar 382355, India
[3]Department of Environmental Geochemical Cycle Research, JAMSTEC, Yokohama, 2360001, Japan

Correspondence to: Shyam Lal (shyam@prl.res.in)

Abstract. About 70 % of the anthropogenic carbon dioxide (CO_2) is emitted from the megacities and urban areas of the world. In order to draw effective emission mitigation policies for combating future climate change as well as independently validating the emission inventories for constraining their large range of uncertainties, especially over major metropolitan areas of developing countries, there is an urgent need for greenhouse gas measurements over representative urban regions. India is a fast developing country, where fossil fuel emissions have increased dramatically in the last three decades and are predicted to continue to grow further by at least 6 % per year through to 2025. The CO_2 measurements over urban regions in India are lacking. To overcome this limitation, simultaneous measurements of CO_2 and carbon monoxide (CO) have been made at Ahmedabad, a major urban site in western India, using a state-of-the-art laser-based cavity ring down spectroscopy technique from November 2013 to May 2015. These measurements enable us to understand the diurnal and seasonal variations in atmospheric CO_2 with respect to its sources (both anthropogenic and biospheric) and biospheric sinks. The observed annual average concentrations of CO_2 and CO are 413.0 ± 13.7 and 0.50 ± 0.37 ppm respectively. Both CO_2 and CO show strong seasonality with lower concentrations (400.3 ± 6.8 and 0.19 ± 0.13 ppm) during the south-west monsoon and higher concentrations (419.6 ± 22.8 and 0.72 ± 0.68 ppm) during the autumn (SON) season. Strong diurnal variations are also observed for both the species. The common factors for the diurnal cycles of CO_2 and CO are vertical mixing and rush hour traffic, while the influence of biospheric fluxes is also seen in the CO_2 diurnal cycle. Using CO and

CO_2 covariation, we differentiate the anthropogenic and biospheric components of CO_2 and found significant contributions of biospheric respiration and anthropogenic emissions in the late night (00:00–05:00 h, IST) and evening rush hours (18:00–22:00 h) respectively. We compute total yearly emissions of CO to be 69.2 ± 0.07 Gg for the study region using the observed $CO : CO_2$ correlation slope and bottom-up CO_2 emission inventory. This calculated emission of CO is 52 % larger than the estimated emission of CO by the emissions database for global atmospheric research (EDGAR) inventory. The observations of CO_2 have been compared with an atmospheric chemistry-transport model (ACTM), which incorporates various components of CO_2 fluxes. ACTM is able to capture the basic variabilities, but both diurnal and seasonal amplitudes are largely underestimated compared to the observations. We attribute this underestimation by the model to uncertainties in terrestrial biosphere fluxes and coarse model resolution. The fossil fuel signal from the model shows fairly good correlation with observed CO_2 variations, which supports the overall dominance of fossil fuel emissions over the biospheric fluxes in this urban region.

1 Introduction

Carbon dioxide (CO_2) is the most important anthropogenically emitted greenhouse gas (GHG) and has increased substantially from 278 to 390 parts per million (ppm) in the atmosphere since the beginning of the industrial era (circa 1750). It has contributed to more than 65 % of the radiative forcing increase since 1750 and hence leads to a signif-

icant impact on the climate system (Ciais et al., 2013). Major causes of CO$_2$ increase are anthropogenic emissions, especially fossil fuel combustion, cement production and land use change. Land and oceans are the two important sinks of atmospheric CO$_2$, which remove about half of the anthropogenic emissions (Le Quéré et al., 2014). The prediction of future climate change and its feedback rely mostly on our ability to quantify fluxes of greenhouse gases, especially CO$_2$, at regional (100–1000 km^2) and global scales. Though the global fluxes of CO$_2$ can be estimated fairly well, the regional-scale fluxes are associated with quite high uncertainty especially over southern Asia; the estimation uncertainty being larger than the value itself (Patra et al., 2013; Peylin et al., 2013). Detailed scientific understanding of the flux distributions is also needed for formulating effective mitigation policies.

Along with the need for atmospheric measurements for predicting future levels of CO$_2$, quantifying the components of anthropogenic emissions of CO$_2$ is likewise important for providing an independent verification of mitigation strategies as well as understanding the biospheric component of CO$_2$. CO$_2$ measurements alone would not be helpful due to the large role of biospheric fluxes in its atmospheric distributions. The proposed strategy for the quantification of the anthropogenic component of CO$_2$ emissions is to simultaneously measure the anthropogenic tracers (Duren and Miller, 2012). CO can be used as a surrogate tracer for detecting and quantifying anthropogenic emissions from burning processes, since it is a major product of incomplete combustion (Turnbull et al., 2006; Wang et al., 2010; Duren and Miller, 2012). The vehicular as well as industrial emissions contribute large fluxes of CO$_2$ and CO to the atmosphere in urban regions. Several simultaneous ground-based and aircraft-based studies of CO and CO$_2$ have been carried out in the past in different parts of the world (Turnbull et al., 2006; Wunch et al., 2009; Wang et al., 2010; Newman et al., 2013) but such a study has not been done in India except for recently reported results from weekly samples for three Indian sites by Lin et al. (2015).

Measurements in different regions (e.g. rural, remote, urban) and at different frequencies (e.g. weekly, daily, hourly) have their own advantages and limitations. For example, taking measurements at remote locations at weekly intervals can be useful for studying seasonal cycles, growth rates and estimating the regional carbon sources and sinks after combining their concentrations with inverse modelling and atmospheric tracer transport models. However, some important studies, like on diurnal variations, temporal covariance etc., are not possible from these measurements due to their limitations. An analysis on temporal covariance of atmospheric mixing processes and variation of flux along shorter timescales, e.g. sub-daily, is essential for understanding local-to-urban scale CO$_2$ flux variations (Ahmadov et al., 2007; Pérez-Landa et al., 2007; Briber et al., 2013; Lopez et al., 2013; Ammoura et al., 2014; Ballav et al., 2015). Urban regions contribute

about 70 % of global CO$_2$ emissions from anthropogenic sources and are projected to increase further over the coming decades (Duren and Miller, 2012). Hence, measurements over these regions are very helpful for understanding emissions growth as well as verifying the mitigation policies. The first observations of CO$_2$, CO and other greenhouse gases started in February 1993 from Cape Rama (CRI: a clean site) on the south-west coast of India using flask samples (Bhattacharya et al., 2009). Since then, several other groups have initiated the measurements of surface-level greenhouse gases (Mahesh et al., 2014; Sharma et al., 2014; Tiwari et al., 2014; Lin et al., 2015). Most of these measurements are made at weekly or fortnightly time intervals. Two aircraft-based measurement programmes, namely, Civil Aircraft for the regular Investigation of the atmosphere Based on an Instrument Container (CARIBIC) (Brenninkmeijer et al., 2007) and Comprehensive Observation Network for TRace gases by AIrLiner (CONTRAIL) (Machida et al., 2008) have provided an important first look at the southern Asian CO$_2$ budget, but these data have their own limitations (Patra et al., 2011; Schuck et al., 2010, 2012). It is pertinent to mention here that until now, there have been no reports of CO$_2$ measurements over an urban location in India. Sampling the urban regions could be very useful for understanding the role of the Indian subcontinent in the global carbon budget as well as for mitigation purpose, since anthropogenic activities are growing strongly over this region. Hence, the present study is an attempt to reduce this gap by understanding the CO$_2$ levels in light of its sources and sinks at an urban region in India.

In view of the above, simultaneous continuous measurements of CO$_2$ and CO have been made since November 2013 from an urban site, Ahmedabad, located in western India, using a highly sensitive laser-based technique. The preliminary results of these measurements for a 1-month period have been reported in Lal et al. (2015). These detailed measurements are utilized for studying the temporal variations (diurnal and seasonal) of both gases, their emission characteristics on diurnal and seasonal scales using their mutual correlations, estimating the contribution of anthropogenic and biospheric emission components in the diurnal cycle of CO$_2$ using the ratio of CO to CO$_2$ and roughly estimating the annual CO emissions from the study region. Finally, the measurements of CO$_2$ have been compared with simulations using an atmospheric chemistry-transport model to discuss roles of various processes contributing to CO$_2$ concentration variations.

2 Site description, local emission sources and meteorology

The measurement facility is housed inside the campus of the Physical Research Laboratory (PRL), situated in the western part of Ahmedabad (23.03° N, 72.55° E, 55 m a.m.s.l.) in the state of Gujarat, India (Fig. 1). It is a semi-arid, urban
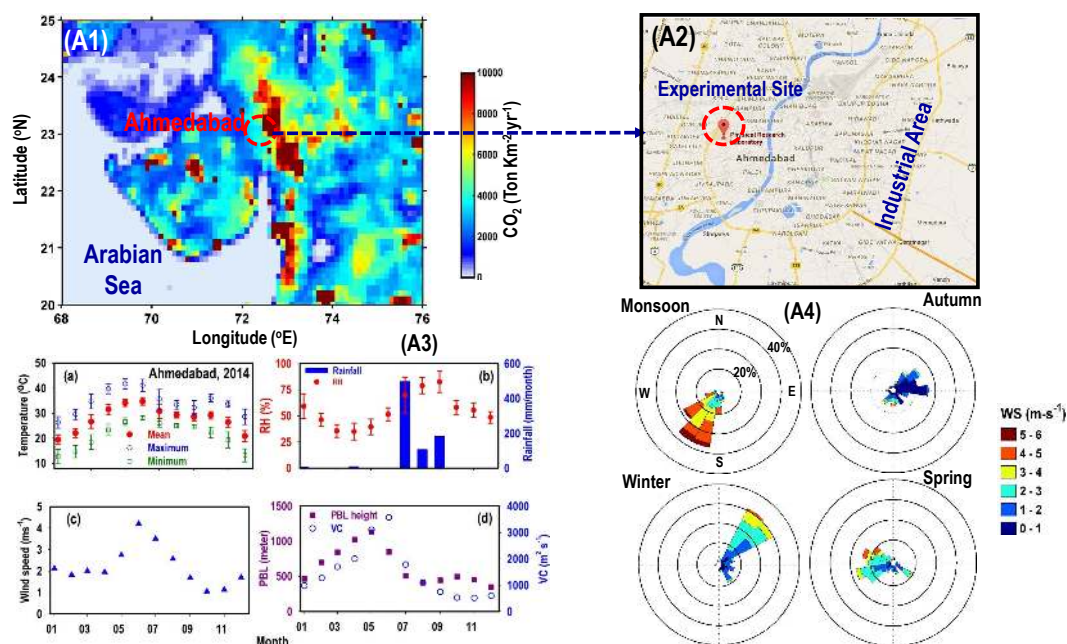
Figure 1. (A1) Spatial distribution of total anthropogenic CO$_2$ emissions from the EDGARv4.2 inventory over Ahmedabad and surrounding regions. **(A2)** The Ahmedabad city map showing location of the experimental site (PRL). **(A3**: a–d) Monthly average temperature with monthly maximum and minimum values, relative humidity (RH), rainfall, wind speed, PBL height and ventilation coefficient (VC) over Ahmedabad during the year 2014. Temperature, RH and wind speed are taken from Wunderground weather (www.wunderground.com), while rainfall and PBLH data are used from the Tropical Rainfall Measuring Mission (TRMM) satellite and MERRA reanalysis data. **(A4)** Wind rose plots for Ahmedabad for the four seasons of 2014 using daily averaged data from Wunderground.

region in western India and has a variety of large- and small-scale industries (textile mills and pharmaceutical companies) in the eastern and northern outskirts. The institute is situated about 15–20 km away from these industrial areas and surrounded by trees on all sides. The western part is dominated by the residential areas. The city has a population of about 5.6 million (Census India, 2011) and has a large number of automobiles (about 3.2 million), which are increasing at the rate of about 10 % per year. Most of the city buses and auto-rickshaws (three-wheelers) use compressed natural gas (CNG) as fuel. The transport-related activities are the major contributors of various pollutants (Mallik et al., 2015). An emission inventory for this city, which has been developed for all known sources, shows the annual emissions (for year 2010) of CO$_2$ and CO at about 22.4 million tons and 707 000 tons respectively (http://www.indiaenvironmentportal.org.in/files/file/Air-Pollution-in-Six-Indian-Cities.pdf). Of these emissions, the transport sector contributes about 36 % in CO$_2$ emissions and 25 % in CO emissions, power plants contribute about 32 % in CO$_2$ emissions and 30 % in CO emissions, industries contribute about 18 % in CO$_2$ emissions and 12 % in CO emissions and domestic sources contribute about 6 % in CO$_2$ emissions and 22 % in CO emissions. The Indo-Gangetic Plain (IGP), situated to the north-east of Ahmedabad, is a very densely populated region and has high levels of

pollutants, emitted from various industries and power plants along with anthropogenic emissions from fossil fuels and traditional biofuels (wood, cow-dung cake etc.). The Thar Desert and the Arabian Sea are situated to the north-west and south-west of Ahmedabad respectively.

Figure 1 shows the average monthly variability of temperature, relative humidity (RH) and wind speed data taken from Wunderground (http://www.wunderground.com); rainfall data from Tropical Rainfall Measuring Mission (TRMM) and planetary boundary layer height (PBLH) data from the Modern-era Retrospective Analysis for Research and Applications (MERRA). The wind rose plot shows the surface-level wind speed and direction during different seasons over Ahmedabad in 2014. Large seasonal variations are observed in the wind speed and direction over Ahmedabad. During the summer monsoon season (June–July–August), the intertropical convergence zone (ITCZ) moves northwards across India. It results in the transport of moist and cleaner marine air from the Arabian Sea and Indian Ocean to the study location by south-westerly winds or the so-called south-west monsoon (summer monsoon). The first shower due to the onset of the south-west monsoon occurs in July and retreats in mid-September over Ahmedabad. Due to heavy rain and winds, mostly from the oceanic region, RH shows higher values in July, August and September. The highest RH value of about 83 % is observed in September. The long-range trans-

port of air masses from the north-eastern part of the Asian continent starts to prevail over India when ITCZ moves back southwards in September and October. These months are regarded as a transition period for the monsoon. During autumn (September–October–November), the winds are calm and undergo a change in their direction from south-west to north-east. When the transition of winds from the oceanic to the continental region takes place in October, the air gets dryer and RH decreases until December. The winds are north-easterly during winter (December–January–February) and transport pollutants mostly from continental region (IGP region). During the spring season (March–April–May), winds are north-westerly and a little south-westerly which transport mixed air masses from continent and oceanic regions. The average wind speed is observed higher in June and July while lower in October and March when transition of wind starts from oceanic to continental and continental to oceanic region respectively. The monthly averaged temperature starts increasing from January and attains maximum (34.6 ± 1.4 °C) in June, followed by a decrease until September and temperature is slightly warmer in October compared to the adjacent months. The monthly variation in planetary boundary layer height (PBLH) closely resembles the temperature pattern. Maximum PBLH of about 1130 m is found in June and it remains in the lower range at about 500 m during July to January. The ventilation coefficient (VC) is obtained by multiplying wind speed and PBL height, which gradually increases from January and attains the maximum value in June, followed by a decrease until November.

3 Experiment and model details

3.1 Experimental method

The ambient measurements of CO_2 and CO concentrations have been made using the wavelength-scanned cavity ring down spectroscopic technique (CRDS)-based analyser (Picarro-G2401) at 0.5 Hz. CRDS offers highly sensitive and precise measurements of trace gases in the ambient air, due to its three main characteristics (Bitter et al., 2005; Chen et al., 2010; Karion et al., 2013). (1) It provides very long sample interaction path length (around 20 km), by utilizing a 3-mirror configuration, which enhances its sensitivity over other conventional techniques like Non-dispersive Infrared Spectroscopy (NDIR) and Fourier Transform Infrared Spectroscopy (FTIR). (2) The operating low pressure (140 Torr) of cell allows to isolate a single spectral feature with a resolution of 0.0003 cm^{-1}, which ensures that the peak height or area is linearly proportional to the concentration. (3) The measurements of trace gases using this technique are achieved by measuring the decay time of light intensity inside the cavity while the conventional optical absorption spectroscopy technique is based on absorption of light intensity. Hence, it increases the accuracy of measure-

ments because it is insensitive to the fluctuations of incident light. The cell temperature of the analyser is maintained at 45 °C throughout the study period.

Figure 2 shows the schematic diagram of the experimental set-up, which consists of the analyser, a glass bulb, a Nafion dryer, a heatless dryer, other associated pumps and a set of calibration mixtures. Atmospheric air is sampled continuously from the terrace of the building (25 m a.g.l.) through 1/4 inch PFA Teflon tube via a glass manifold. An external pump is attached on one side of the glass manifold to flush the sample line. Water vapour affects the measurements of CO_2 by diluting its mole fractions in the air and by broadening the spectroscopic absorption lines of other gases. Although, the instrument has the ability to correct for the water vapour interference using an experimentally derived water vapour correction algorithms (Crosson, 2008), but it has an absolute H_2O uncertainty of ~ 1 % (Chen et al., 2010) and can introduce a source of error using a single water vapour correction algorithm (Welp et al., 2013). This error can be minimized either by generating the correction coefficients periodically in the laboratory or by removing the water vapour from the sample air. Conducting the water vapour correction experiment is bit tricky and needs extra care as discussed by Welp et al. (2013). Hence, we prefer to remove water vapour from the sample air by introducing a 50-strand Nafion dryer (Perma Pure, p/n PD-50T-24MSS) upstream of the analyser. The Nafion dryer contains a bunch of semipermeable membrane tubing separating an internal sample gas stream from a counter sheath flow of dry gas in stainless steel outer shell. The partial pressure of water vapour in the sheath air should be lower than the sample air for effectively removing the water vapour from the sample air. A heatless dryer generates dry air using a 4-bar compressor (KNF, MODEL: NO35ATE), which is used as a sheath flow in the Nafion dryer. After drying, sample air passes through the PTFE filter (polytetrafluoroethylene; 5 µm Sartorius AG, Germany) before entering the instrument cavity. This set-up dries the ambient air near to 0.03 % (300 ppm) concentration of H_2O.

The measurement system is equipped with three high-pressure aluminium cylinders containing gas mixtures of CO_2 (350.67 ± 0.02, 399.68 ± 0.01 and 426.20 ± 0.01 ppm) in dry air from NOAA, Bolder USA, and one cylinder of CO (970 parts per billion (ppb)) from Linde UK. These tanks were used to calibrate the instrument for CO_2 and CO. An additional gas standard tank (CO_2: 338 ppm, CO: 700 ppb), known as the "target", is used to monitor the instrumental drift and to assess the data set accuracy and repeatability. The target tank values are calibrated against the CO_2 and CO calibration mixtures. The target tank and calibration gases were usually measured in the middle of every month (Each calibration gas is passed for 30 min and the target tank for 60 min). The target gas is introduced into the instrument for a period of 24 h once every six months, for checking the diurnal variability of instrument drift. Maximum drift for 24 h
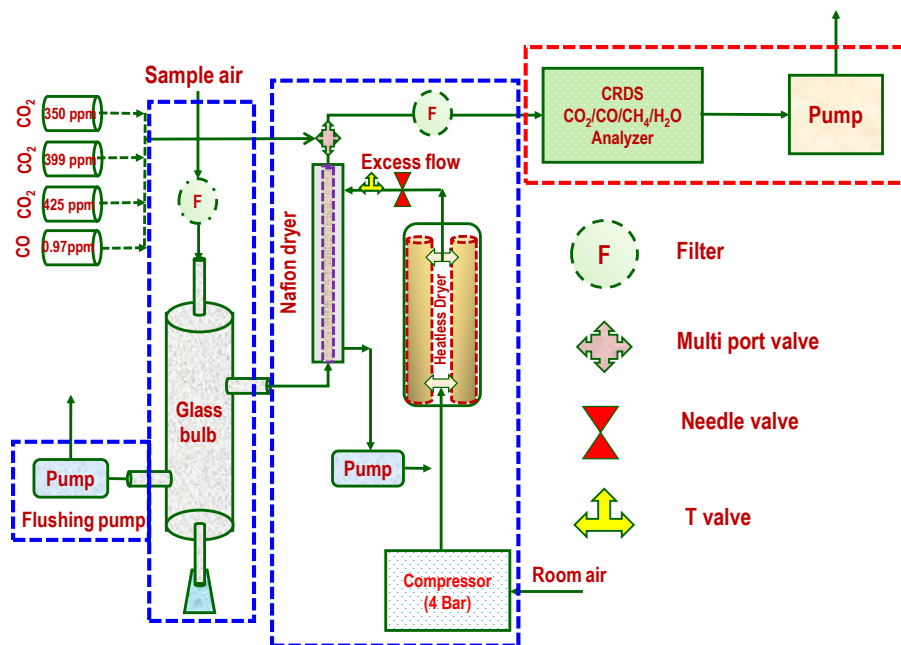
Figure 2. Schematic diagram of the experimental set-up. We additionally introduce a Nafion dryer upstream of the inlet of the instrument for removing the water vapour. Three calibration mixtures from NOAA, USA are used to calibrate CO_2 measurements and one calibration mixture from Linde, UK is used to calibrate CO measurements. The red-coloured box covers the analyser system received from the company, while two blue-coloured boxes cover the 2-stage moisture-removing systems, designed at our lab in PRL.

has been calculated by subtracting the maximum and minimum values of 5 min averages, which were found to be 0.2 and 0.015 ppm for CO_2 and CO. For all calibration mixtures, the measured concentration is calculated as the average of the last 10 min. The linearity of the instrument for CO_2 measurements has been checked by applying the linear fit equation of the CO_2 concentration of the calibration standards (350.67, 399.68 and 426.20 ppm), measured by the analyser. The slope is found in the range of 0.99–1.007 with a correlation coefficient (r) of about 0.999. Further, linearity of the instrument for CO is also checked by diluting the calibration mixture from 970 to 100 ppb. The calibration mixture is diluted with pure air (free from water vapour, particles, carbon monoxide (CO), sulphur dioxide (SO_2), oxides of nitrogen (NO_x), ozone (O_3) and hydrocarbons (HC)) from an ECO Physics zero-air generator. The flows of calibration mixture and pure air were regulated using two separate mass flow controllers from Aalborg. For increasing the interaction times of the gases (zero air and calibration mixture) and to ensure a homogeneous mixing, the spring-shaped dead volume is used. Each diluted mixture is passed for 30 min in the instrument and the data averaged from the last 10 min is used. The instrument shows excellent linearity for CO and the slope is observed to be 0.98. The accuracy of the measurements is calculated by subtracting the mean difference of measured CO_2 and CO concentrations from the actual concentration of both gases in target gas. The accuracies of CO_2 and CO are found to be in the range of 0.05–0.2 ppm and

0.01–0.025 ppm respectively. The repeatability of both gases are calculated using the standard deviation of the mean concentration of target gas measured by the analyser over the period of observations and found to be 0.3 and 0.04 ppm for CO_2 and CO respectively.

3.2 Description of AGCM-based chemistry-transport model (ACTM)

This study uses the Center for Climate System Research/National Institute for Environmental Studies/Frontier Research Center for Global Change (CCSR/NIES/FRCGC) atmospheric general circulation model (AGCM)-based chemistry-transport model (ACTM). The model is nudged with reanalysis meteorology using a Newtonian relaxation method. The U and V components of horizontal winds are from the Japan Meteorological Agency Reanalysis (JRA-25; Onogi et al., 2007). The model has $1.125° \times 1.125°$ horizontal resolution (T106 spectral truncation) and 32 vertical sigma-pressure layers up to about 50 km. Three components, namely anthropogenic emissions, monthly varying ocean exchange with net uptake and terrestrial biospheric exchange of surface CO_2 fluxes are used in the model. The fossil fuel emissions are taken from the EDGAR inventory for the year 2010. Air–sea fluxes from Takahashi et al. (2009) have been used for the oceanic CO_2 tracer. The oceanic fluxes are monthly and are linearly interpolated between mid-months. The terrestrial biospheric CO_2 tracers are provided by the

Carnegie–Ames–Stanford approach (CASA) process model (Randerson et al., 1997), after introducing a diurnal variability using 2 m air temperature and surface short wave radiation from the JRA-25 as per Olsen and Randerson (2004). The ACTM simulations have been extensively used in TransCom CO$_2$ model intercomparison studies (Law et al., 2008; Patra et al., 2008).

4 Results and discussion

4.1 Time series and general statistics

Figure 3a and c show the time series of 30 min averaged CO$_2$ and CO concentrations for the periods from November 2013 to February 2014 and July 2014 to May 2015. Large and periodic variations indicate the stronger diurnal dependence of the gases. Concentrations and variability of both gases were observed at their lowest in the months of July and August, while maximum scatter in the concentrations and several plumes with very high levels of the gases have been observed from October 2014 to mid-March 2015. Almost all plumes of CO$_2$ and CO have one-to-one correlations and are mostly found during evening and late night rush hours. Figure 3e and f show the variations of CO$_2$ and CO concentrations with wind speed and direction for the study period except for July, August and September, due to non-availability of wind data. Most of the high and low concentrations of the gases are found to be associated with low and high wind speeds. There is no specific direction associated with the high levels of these gases. This probably indicates that the transport sector is an important contributor to local emissions since the measurement site is in the midst of an urban city.

Figure 3b and d show the probability distributions or frequency distributions of CO$_2$ and CO concentrations during the study period. Both gases show different distributions from each other. This difference could be attributed to the additional impact of the biospheric cycle (photosynthesis and respiration) on the levels of CO$_2$ apart from the common controlling factors (local sources, regional transport, PBL dynamics etc.) responsible for distributions of both gases. The control of the boundary layer is common for the diurnal variations of these species because their chemical lifetimes are longer ($>$ months) than the timescale of PBL height variations ($\sim$ h). However, biospheric fluxes of CO$_2$ can have strong hourly variations. During the study period the CO$_2$ concentrations varied between 382 and 609 ppm, with 16 % of data lying below 400 ppm, 50 % lying in the range 400–420 ppm, 25 % between 420 and 440 ppm and 9 % in the range of 440–570 ppm. Maximum frequency of CO$_2$ is observed at 402.5 ppm during the study period. The CO concentrations lies in the range of 0.071–8.8 ppm with almost 8 % of data lying below the most probable frequency of CO at 0.2 ppm, while 70 % of data lies between the concentrations of 0.21 and 0.55 ppm. Only 8 % of data lies

above the concentration of 1.6 ppm and the remaining 14 % lies between 0.55 and 1.6 ppm. The annual mean concentrations of CO$_2$ and CO are found to be 413.0 ± 13.7 ppm and 0.50 ± 0.37 ppm respectively, after removing outliers beyond 2σ values.

4.2 Seasonal variations of CO$_2$ and CO

The seasonal cycles of CO$_2$ and CO are mostly governed by the strength of emission sources, sinks and transport patterns. They follow almost identical seasonal patterns, but the factors responsible for their seasonal behaviours are distinct. We calculate the seasonal cycles of CO$_2$ and CO using two different approaches. In the first approach, we use the monthly mean of all measurements and in the second approach we only use the monthly mean of measurements from the afternoon period (12:00–16:00 h). The seasonal cycles from the first approach will present the overall variability in both gases. On the other hand, the second approach removes the auto-covariance by excluding CO$_2$ and CO data mainly affected by local emission sources and represent seasonal cycles at the well-mixed volume of the atmosphere. The CO$_2$ time series is detrended by subtracting a mean growth rate of CO$_2$ observed at Mauna Loa (MLO), Hawaii, i.e. 2.13 ppm year^{-1} or 0.177 ppm month^{-1} (www.esrl.noaa.gov/gmd/ccgg/trends/) for clearly depicting the seasonal cycle amplitude. Figure 4a and b show the variations of monthly average concentrations of CO$_2$ and CO using all daily (0–24 h) data and afternoon (12:00–16:00 h) data.

In general, total mean values of CO$_2$ and CO are observed to be lower in July, having concentrations of 398.78 ± 2.8 and 0.15 ± 0.05 ppm respectively. During summer monsoon months the predominance of south-westerly winds, which bring cleaner air from the Arabian Sea and the Indian Ocean over to Ahmedabad (Fig. 1), and high VC are mostly responsible for the lower concentration of the total mean of both gases. CO$_2$ and CO concentrations are also at their seasonal low in the northern hemisphere due to net biospheric uptake of CO$_2$ and seasonally high chemical loss of CO through reaction with OH. In addition to this, deep convection efficiently transports the emitted pollutants (CO, hydrocarbons.etc) and biospheric uptake signals (of CO$_2$) from the surface to the upper troposphere during the summer monsoon, resulting in lower concentrations at the surface in the summer compared to the winter months (Kar et al., 2004; Randel and Park, 2006; Park et al., 2009; Patra et al., 2011; Baker et al., 2012). During autumn and early winter (December), lower VC caused trapping of anthropogenically emitted CO$_2$ and CO, and is the major cause for high concentrations of both gases during this period. In addition to this, wind changes from the cleaner marine region to the polluted continental region, especially from the IGP region, could be an additional factor for higher levels of CO$_2$ and CO during these seasons (autumn and winter). Elevated levels during these
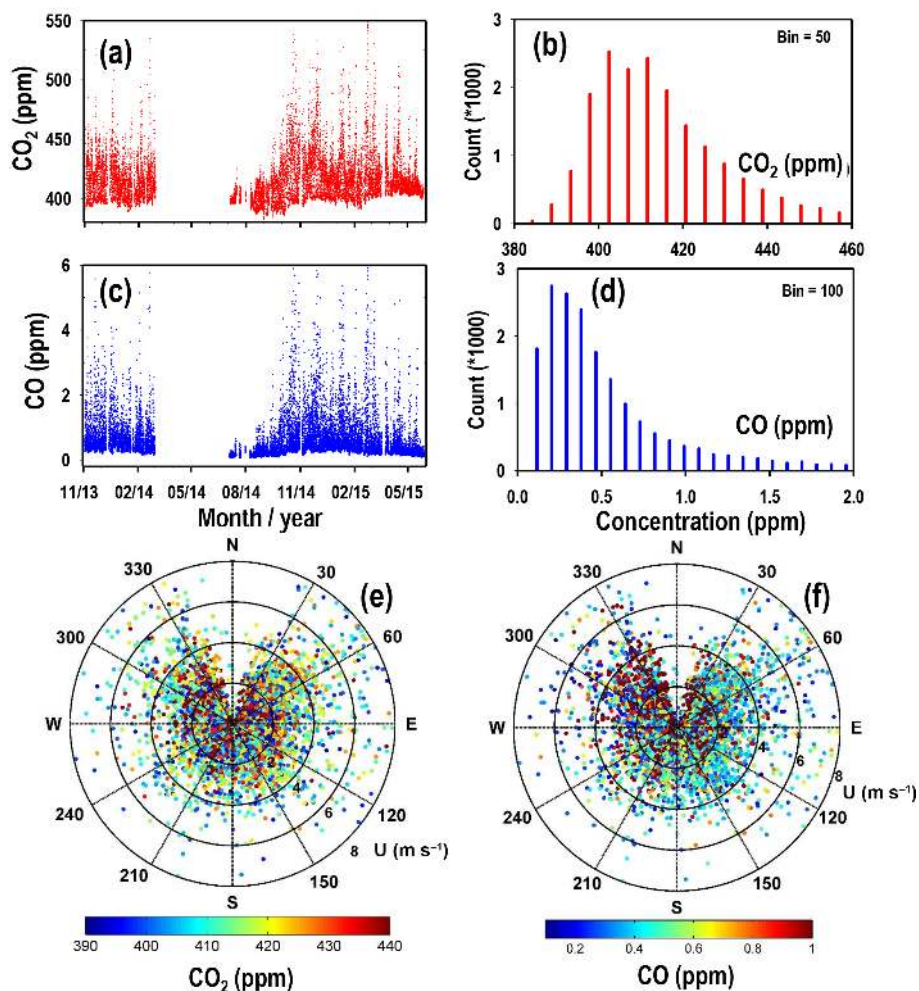
Figure 3. (a, c) Time series of 30 min averaged values of CO_2 and CO measured at Ahmedabad for the study period. **(b, d)** The frequency distribution in CO_2 and CO concentrations for the study period using a 30 min mean of the gases. **(e, f)** The polar plots show the variation of 30 min averaged CO_2 and CO at this site with wind direction and speed during the study period except July, August and September due to unavailability of meteorology data.

seasons are also examined in several other pollutants over Ahmedabad as discussed in previous studies (Sahu and Lal, 2006; Mallik et al., 2016). Maximum concentrations of CO_2 and CO are observed to be 424.8 ± 17 and 0.83 ± 0.53 ppm respectively during November. From January to May the total mean concentration of CO_2 decreases from 415.3 ± 13.6 to 406.1 ± 5.0 ppm and total mean concentration of CO decreases from 0.71 ± 0.22 to 0.22 ± 0.10 ppm. Higher VC and predominance of comparatively less polluted mixed air masses from oceanic and continental region result in lower concentrations of both gases during this period. There are some clear differences which are observed in the afternoon mean concentrations of CO_2 compared to daily mean. The first distinctive feature is that a significant difference of about 5 ppm is observed in the afternoon mean of CO_2 concentrations from July to August compared to the difference in total mean concentrations of about ~ 0.38 ppm for the same

period. Significant differences in the afternoon concentrations of CO_2 from July to August are mainly due to the increasing sink by net biospheric productivity after the Indian summer monsoonal rainfall. Another distinct feature is that the daily mean concentration of CO_2 is found to be highest in November, while the afternoon mean concentration of CO_2 attains maximum value (406 ± 0.4 ppm) in April. A prolonged dry season combined with high daytime temperatures (about $41\,^\circ$C) during April–May create a tendency for the ecosystem to become a moderate source of carbon exchange (Patra et al., 2011) and this could be responsible for the elevated mean noontime concentrations of CO_2. Unlike CO_2, seasonal patterns of CO from total and afternoon mean concentrations are identical, although levels are different. It shows that the concentrations of CO are mostly governed by identical sources during day- and night-time throughout the year.

The average amplitude (max–min) of the annual cycle of CO$_2$ is observed at around 13.6 and 26.07 ppm from the afternoon mean and total mean respectively. Different annual cycles and amplitudes have been observed from other studies conducted over different Indian stations. Similarly to our observations of the afternoon mean concentrations of CO$_2$, maximum values are also observed in April at Pondicherry (PON) and Port Blair (POB) with amplitudes of mean seasonal cycles at about 7.6 ± 1.4 and 11.1 ± 1.3 ppm respectively (Lin et al., 2015). Cape Rama (CRI), a costal site on the south-west coast of India shows seasonal maxima one month before our observations in March with an annual amplitude of about 9 ppm (Bhattacharya et al., 2009). The Sinhagad (SNG) site located over the Western Ghats mountain range, show much larger seasonal cycles with annual amplitude at about 20 ppm (Tiwari et al., 2014). The amplitude of the mean annual cycle at the free tropospheric site, Hanle, at an altitude of 4500 m is observed to be 8.2 ± 0.4 ppm, with maxima in early May and minima in mid-September (Lin et al., 2015). Distinct seasonal amplitudes and patterns are due to differences in regional controlling factors for the seasonal cycle of CO$_2$ over these locations, e.g. Hanle is remotely located from all continental sources, at the Port Blair site predominantly marine air is sampled, Cape Rama observes marine air in the summer and Indian flux signals in the winter, and Sinhagad represents a forested ecosystem. These comparisons show the need for CO$_2$ measurements over different ecosystems for constraining its budget.

The annual amplitudes in afternoon and daily mean CO concentrations are observed to be about 0.27 and 0.68 ppm. The seasonal cycle of CO over PON and POB shows a maximum in the winter months and minimum in the summer months with annual amplitudes of 0.078 ± 0.01 and 0.144 ± 0.016 ppm respectively, which are similar to our results. So the seasonal levels of CO are affected by large-scale dynamics, which changes air masses from marine to continental and vice versa, and by photochemistry. The amplitudes of annual cycles at these locations differ due to their climatic conditions and source/sink strengths.

4.3 Diurnal variation

The diurnal patterns for all months and seasons are produced by first generating the time series from the 15 min averages and then averaging the individual hours for all days of the respective month and season after removing the values beyond 2σ standard deviations for each month as outliers.

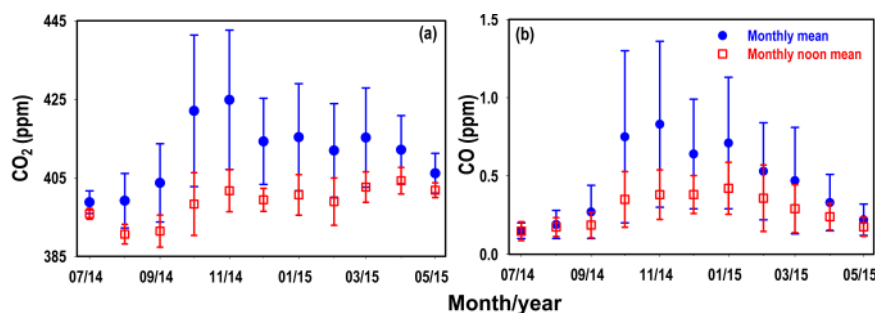### 4.3.1 Diurnal variation of CO$_2$

Figure 5a shows the mean diurnal cycles of atmospheric CO$_2$ and associated 1σ standard deviation (shaded region) during all four seasons. All times are in Indian Standard Time (IST), which is 5.5 h ahead of Universal Time (UT). Noticeable differences are observed in the diurnal cycle of CO$_2$ from

season to season. In general, maximum concentrations have been observed during morning (07:00–08:00) and evening (18:00–20:00) hours, when PBL is shallow, traffic is dense and vegetation respiration dominates due to the absence of photosynthesis activity. The minimum of the cycles occurs in the afternoon hours (14:00–16:00) when PBL is deepest and well mixed, as well as when vegetation photosynthesis is active. There are many interesting features in the period of 00:00–08:00. CO$_2$ concentrations start decreasing from 00:00 to 03:00 and increase slightly afterwards until 06:00–07:00 during summer and autumn. Respiration of CO$_2$ from vegetation is mostly responsible for this night-time increase. During winter and spring seasons CO$_2$ levels are observed constant during night hours and small increase is observed only from 06:00 to 08:00 during the winter season. In contrast to this, the subsequent section shows a continuous decline in the night-time concentrations of the main anthropogenic tracer CO, which indicates that there is enough vertical mixing of low CO air from above that once the CO source is turned off, its concentration drops. Hence, constant levels of CO$_2$ at night during these seasons give evidence of a continued but weak source (such as respiration) in order to offset dilution from mixing low CO$_2$ air from aloft. Dry soil conditions could be one of the possible causes of weak respirations. Further, distinct timings have been observed in the morning peak of CO$_2$ during different seasons. It is mostly related to the sunrise time, which decides the evolution time of PBL height and the beginning of vegetation photosynthesis. Sunrise occurs at 05:55–06:20, 06:20–07:00, 07:00–07:23 and 07:20–05:54 during summer, autumn, winter and spring respectively. During spring and summer, rush hour starts after sunrise, so the vehicular emissions occur when the PBL has been already high and photosynthetic activity has begun. The CO$_2$ concentration is observed lowest in the morning during the summer monsoon season compared to other seasons. This is because CO$_2$ uptake by active vegetation deplete entire mixed layer during daytime and when the residual layer mixes to the surface in the morning, low-CO$_2$ air is mixed down. In winter and autumn, rush hour starts parallel with the sunrise, so the emissions occur when the PBL is low and hence concentration build-up is much stronger in these seasons than in spring and summer.

The diurnal amplitude is defined as the difference between the maximum and minimum concentrations of CO$_2$ in the diurnal cycle. The amplitudes of a monthly averaged diurnal cycle of CO$_2$ from July 2014 to May 2015 are shown in Fig. 5b. The diurnal amplitude shows large month-to-month variation with increasing trend from July to October and decreasing trend from October onwards. The lowest diurnal amplitude of about 6 ppm is observed in July while the highest amplitude at about 51 ppm is observed in October. The amplitude does not change largely from December to March and is observed in the range of 25–30 ppm. Similarly from April to May the amplitude varies in a narrow range from 12 to 15 ppm. The jump in the amplitude of the CO$_2$ diurnal cy-

Figure 4. The seasonal variation of CO_2 and CO from July 2014 to May 2015 using their monthly mean concentrations. The blue dots and red rectangles show the monthly average concentrations of these gases for the total (0–24 h) and noontime (12:00–16:00) data respectively with 1σ spread.
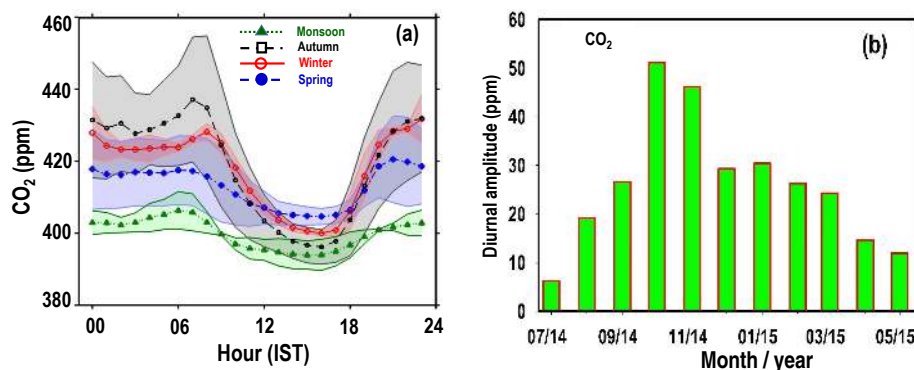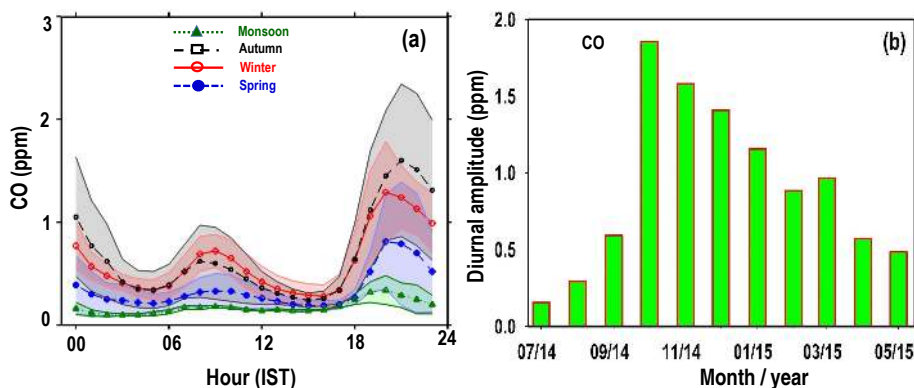

Figure 5. (a) Average diurnal variation of CO_2 over Ahmedabad during all four seasons. **(b)** Monthly variation of average diurnal amplitude of CO_2 during from July 2014 to May 2015. All times are in Indian Standard Time (IST), which is 5.5 h ahead of Universal Time (UT).

cle is observed to be highest (around 208 %) from July to August. This is mainly due to a significant increase in biospheric productivity from July to August after the rains in Ahmedabad. It is observed that during July the noontime CO_2 levels are found in the range of 394–397 ppm, while in August the noontime levels are observed in the range of 382–393 ppm. The lower levels could be due to the higher PBL height during the afternoon and the cleaner air, but in the case of CO (to be discussed in next section), average daytime levels in August are observed to be higher than in July. It rules out that the lower levels during August are due to the higher PBL height and presence of cleaner marine air, and confirms the higher biospheric productivity during August.

Near-surface diurnal amplitude of CO_2 has also been documented at the humid subtropical Indian station, Dehradun, and a dry tropical Indian station, Gadanki (Sharma et al., 2014). In comparison to Ahmedabad, both stations show distinct seasonal change in the diurnal amplitude of CO_2. The maximum CO_2 diurnal amplitude of about 69 ppm is observed during the summer season at Dehradun (30.3° N, 78.0° E, 435 m), whereas maximum of about 50 ppm is observed during autumn at Gadanki (13.5° N, 79.2° E, 360 m).

4.3.2 Diurnal variation of CO

Figure 6a shows seasonally averaged diurnal variation of CO. In general, the mean diurnal cycle of CO shows lower concentration during noon (12:00–17:00) and two peaks in the morning (08:00 to 10:00) and in the evening (18:00 to 22:00) hours. This cycle exhibits the same pattern as the mean diurnal cycle of traffic flow, with maxima in the morning and at the end of the afternoon, which suggests the influence of traffic emissions on CO measurements. Along with the traffic flow, PBL dynamics also play a critical role in governing the diurnal cycle of CO. The amplitudes of the evening peak in diurnal cycles of CO are always greater than the morning peaks. It is because the PBL height evolves side by side with the morning rush hour traffic and hence increased dilution, while during evening hours, PBL height decrease along with evening dense traffic and favours the accumulation of pollutants until the late evening under the stable PBL conditions. The noontime minimum of the cycle is mostly associated with the deepest and well-mixed PBL. In general, the average diurnal cycle patterns of both gases (CO_2 and CO) are similar, but have a few noticeable differences. The first difference is observed in the timing of the morning peaks: CO_2 peaks occur slightly before the CO peak due to the triggering

Figure 6. (a) Diurnal variation of CO over Ahmedabad during all four seasons. **(b)** Monthly variation of the diurnal amplitude of CO.
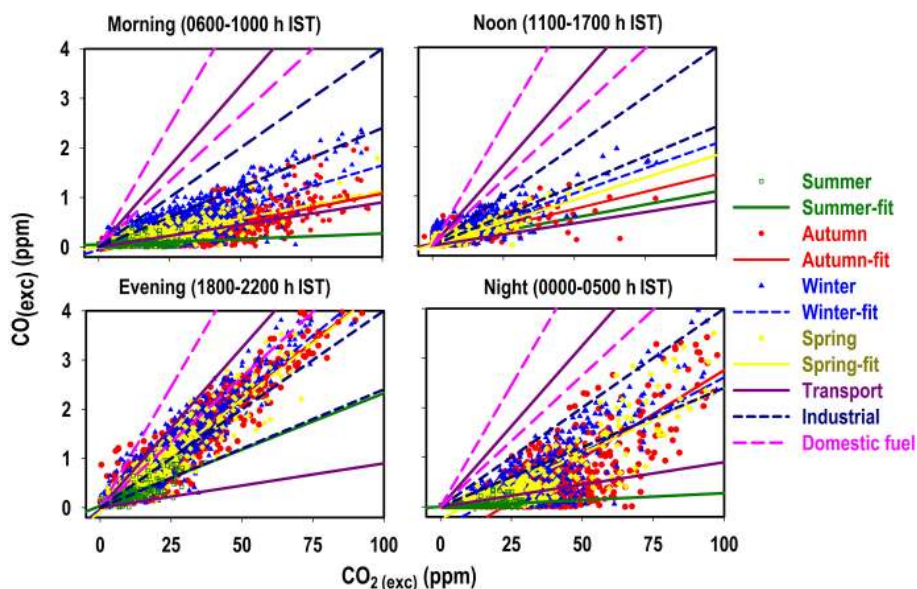
Figure 7. Scatter plots and regression fits of excess CO (CO$_{(exc)}$) vs. excess CO$_2$ (CO$_{2(exc)}$) during morning (06:00–10:00), noon (11:00–17:00), evening (18:00–22:00) and night (00:00–05:00) hours for all four different seasons. Excess values of both species are calculated after subtracting their background concentrations. Each data points are averaged for 30 min. Emission ratios range of CO / CO$_2$ for different sources from the literature are also plotted in each figure.

photosynthesis process by the sunrise. On the other hand, the morning peaks of CO mostly depend on the rush hour traffic and are consistent at 08:00–10:00 in all seasons. The second difference is that the afternoon concentrations of CO show little seasonal spread compared to the afternoon concentrations of CO$_2$. Again, this is due to the biospheric control on the levels of CO$_2$ during the afternoon hours of different seasons, while CO levels are mainly controlled by dilution during these hours. The third noticeable difference is that the levels of CO decrease very fast after evening rush hours in all seasons, while this feature is not observed in the case of CO$_2$ since respiration during night hours contributes to the levels of CO$_2$. The continuous drop of night-time concentrations of CO indicates that there is enough vertical mixing of low CO air from above once the CO source is turned off. The aver-

age morning (08:00–09:00) peak values of CO are observed at a minimum of (0.18 ± 0.1 ppm) in summer and maximum of (0.72 ± 0.16 ppm) in winter, while evening peak shows minimum value (0.34 ± 0.14 ppm) in summer and maximum (1.6 ± 0.74 ppm) in autumn. The changes in CO concentrations show large fluctuations from morning peak to afternoon minima and from afternoon minima to evening peak. From early morning maxima to noon minima, the changes in CO concentrations are found in the range of 20–200 %, while from noon minima to late evening maxima the changes in CO concentrations are found in the range of 85 to 680 %. Similar diurnal variations with two peaks have also been observed in earlier measurements of CO as well as NO$_x$ at this site (Lal et al., 2000).

The evening peak contributes significantly to the diurnal amplitude of CO. The largest amplitude in CO cycle is observed in autumn (1.36 ppm) while the smallest amplitude is observed in summer (0.24 ppm). The diurnal amplitudes of CO are observed to be about 1.01 and 0.62 ppm respectively during winter and spring. Like CO$_2$, the diurnal cycle of CO (Fig. 6b) shows the minimum (0.156 ppm) amplitude in July and maximum (1.85 ppm) in October. After October the diurnal amplitude keeps on decreasing until summer.

4.4 Correlation between CO and CO$_2$

The relationship between CO and CO$_2$ can be useful for investigating the CO source types and their combustion characteristics in the city region of Ahmedabad. The measurements are generally affected by dilution due to the boundary layer dynamics, but their ratios will cancel this effect. Further, the interpretation of correlation ratios in terms of their dominant emission sources needs to isolate first the local urban signal. For this, the measurements have to be corrected from their background influence. The background concentrations are generally those levels which have an almost negligible influence from the local emission sources. The continuous measurements of these gases at a cleaner site can be considered as background data, but due to the unavailability of such measurements for our site and study period, we use the fifth percentile value of CO$_2$ and CO for each day as the background of these gases for the corresponding day. It is observed that the mixing ratios of both gases at low wind speed, which show the influence of local urban signal, are significantly higher than the background levels and hence confirm that the definition of background will not significantly affect the derived ratios (Ammoura et al., 2014). This technique of measuring the background is extensively studied by Ammoura et al. (2014) and found to be suitable for both CO and CO$_2$, even having the role of summer uptake on the levels of CO$_2$. The excess CO$_2$ (CO$_{2(exc)}$) and CO (CO$_{(exc)}$) above the background for Ahmedabad city are determined for each day after subtracting the background concentrations from the hours of each day (CO$_{2(exc)}$ = CO$_{2(obs)}$ − CO$_{2(bg)}$, CO$_{(exc)}$ = CO$_{(obs)}$ − CO$_{(bg)}$).

We use a robust regression method for the correlation study. It is an alternative to the least squares regression method and more applicable for analysing time series data with outliers arising from extreme events (http://www.ats.ucla.edu/stat/stata/dae/rreg.htm). Figure 7 illustrates the correlations between CO$_{(exc)}$ and CO$_{2(exc)}$ for the four seasons at different time windows of the day. Based on the dominance of different atmospheric processes and different emission sources as discussed in Sect. 4.3, the measurements are divided into four different time windows: (1) morning period (06:00–10:00), when PBL height is slowly evolving and rush hour traffic is there, (2) afternoon period (11:00–17:00), when atmosphere is well mixed and traffic volume is relatively low, (3) evening period (18:00–22:00),

when influence of rush hour traffic is significantly high, and (4) night period (00:00–05:00), when the atmosphere is calm and the anthropogenic sources of both gases are switched off. The measured slope values for these time intervals are given in Table 1. The ranges of the emission ratios of CO / CO$_2$ for transport, industrial and domestic sources, as given in Table 2, are also plotted in the figures for broadly showing the dominance of different sources. The $\Delta CO_{(exc)}/\Delta CO_{2(exc)}$ ratios are observed to be lowest during the summer, with a range varying from 0.9 ppb ppm^{-1} in the morning to 19.5 ppb ppm^{-1} in the evening period. The lowest coefficient of determination is also observed during this season, which suggests that the levels of CO and CO$_2$ are controlled by different factors. As discussed previously, higher biospheric productivity during this season mostly controls the CO$_2$ concentrations while CO concentrations are mostly controlled by the long-range transport. During the winter season $\Delta CO_{(exc)}/\Delta CO_{2(exc)}$ ratios are observed at their highest and vary from 14.3 ppb ppm^{-1} in the morning to 47.2 ppb ppm^{-1} in the evening period. Relatively higher ratios during winter compared to the other three seasons indicate a contribution of CO emissions from additional biofuel-burning sources. From day to night, the highest coefficient of determination is observed during spring. As illustrated by the diurnal cycle, CO$_2$ is not significantly removed by the biosphere during spring. Along with this, higher VC during this season will result in very fast mixing. Therefore, very fast mixing will mostly regulate their relative variation and will result in higher correlation in this season. Other factors like soil and plant respiration during this period may also control CO$_2$ concentrations due to which the correlation coefficient is not equal to one. Except for the monsoon, the $\Delta CO_{(exc)}/\Delta CO_{2(exc)}$ ratios and their correlations are fairly comparable in the other seasons in the evening rush hours, which indicates stronger influence of common emission sources. Ratios during this time can be considered as fresh emissions since dilution and chemical loss of CO can be considered negligible for this time. Most of these data fall in the domestic and transport sector emission ratio lines, which indicate that during this time interval these sources mostly dominate (Table 2). On the other hand, during other time intervals most of the data is scattered between emission ratio lines of the industrial and transport sectors. Hence, we can conclude that during evening hours, transport and domestic sources mostly dominate, while during other periods transport and industrial emission sources mostly dominate. The observed ratios are similar to the air mass influenced by both fossil fuel and biofuel emissions as discussed by Lin et al. (2015) over Pondicherry. Using CARIBIC observations, Lai et al. (2010) also reported the $\Delta CO / \Delta CO_2$ ratio in the range of 15.6–29.3 ppb ppm^{-1} from the air mass influenced by both biofuel and fossil fuel burning in the Indochinese Peninsula. Further, the $\Delta CO / \Delta CO_2$ ratio is also observed at about 13 ppb ppm^{-1} in the south-eastern Asian outflow during February–April 2001 during the TRACE-P cam-

Table 1. Correlation slopes ($\Delta CO_{(exc)}/\Delta CO_{2(exc)}$ in ppb ppm^{-1}) measured during different time intervals of distinct seasons. Coefficient of determination (r^2) is given inside the brackets.

Seasons	Slope in ppb ppm^{-1} (Coefficient of determination (r^2)			
	Morning (06:00–10:00)	Afternoon (11:00–17:00)	Evening (18:00–22:00)	Night (00:00–05:00)
Summer (JA)	0.9 (0.15)	10.0 (0.17)	19.5 (0.67)	0.5 (0.16)
Autumn (SON)	8.3 (0.48)	14.1 (0.75)	45.2 (0.90)	35.3 (0.71)
Winter (DJF)	14.3 (0.51)	20.0 (0.68)	47.2 (0.90)	30.0 (0.75)
Spring (MAM)	9.3 (0.68)	18.0 (0.80)	43.7 (0.93)	26.0 (0.80)

paign and it suggests the combined influence of fossil fuel and biofuel burning (Russo et al., 2003). The overall ratios (using all data) from autumn to spring (8.4–12.7 ppb ppm^{-1}) suggest the dominance of local emission sources during these seasons, and this range corresponds to the range of anthropogenic combustion sources (10–15 ppb ppm^{-1}) in developed countries (Suntharalingam et al., 2004; Takegawa et al., 2004; Wada et al., 2011). This suggests that the overall emissions of CO over Ahmedabad are mostly dominated by the anthropogenic combustion during these seasons.

5 Top-down CO emissions from observations

If the emissions of CO_2 are known for a study location, the emissions of CO can be estimated by multiplying the correlation slopes and molecular mass mixing ratios (Wunch et al., 2009; Wong et al., 2015). Final emissions of CO will depend on choosing the values of the correlation slopes. The slopes should not be biased by particular local sources, chemical processing and PBL dynamics. We exclude the summer monsoon season data, as the CO_2 variations mainly depend on the biospheric productivity during this season. As discussed previously, the morning and evening rush hour data are appropriate for tracking vehicular emissions, while the afternoon data are affected by other environmental factors, e.g. the PBL dynamics, biospheric activity and chemical processes. The stable, shallow night-time PBL accumulates emissions since the evening and hence the correlation slope for this period can be used as a signature of the city's emissions. Hence, we calculate the slopes from the data corresponding to the period of night-time (23:00–05:00) and evening rush hour (19:00–22:00). The CO emission (E_{CO}) for Ahmedabad is calculated using the following formula.

$$E_{CO} = \left(\alpha_{CO} \frac{M_{CO}}{M_{CO_2}} \right) E_{CO_2}, \qquad (1)$$

where, α_{CO} is the correlation slope of $CO_{(exc)}$ to $CO_{2(exc)}$ ppb ppm^{-1}, M_{CO} is the molecular mass of CO in g mol^{-1}, M_{CO_2} is the molecular mass of CO_2 in g mol^{-1} and E_{CO_2} is the CO_2 emission in Gigagram (Gg) over Ahmedabad. The EDGARv4.2 emis-

sion inventory reported annual emissions of CO_2 at $0.1° \times 0.1°$ for the period of 2000–2008 (EDGAR Project Team, 2011). It reported an annual CO_2 emission of 6231.6 Gg CO_2 yr^{-1} by EDGARv4.2 inventory over the box (72.3 < longitude < 72.7° E, 22.8 < latitude < 23.2° N) which contain Ahmedabad coordinates in the centre of the box. We assume that the emissions of CO_2 are linearly changing with time, and using increasing rates of emissions from 2005 to 2008, we extrapolate the emissions of CO_2 for 2014 over the same area. The bottom-up CO_2 emissions for Ahmedabad is thus estimated of about 8368.6 Gg for the year 2014. Further, to compare the estimated emissions with inventory emissions, we also extrapolated the CO emissions for the year 2014 using the same method that was applied for CO_2. The slope values and corresponding estimated emissions of CO are given in Table 3.

Further, the uncertainty in total emission due to uncertainty associated with used slope is also calculated. Using this slope and CO_2 emissions from the EDGAR inventory, the estimated fossil fuel emission for CO is observed at 69.2 ± 0.7 Gg (emission $\pm$ uncertainty) for the year 2014. The EDGAR inventory underestimates the emission of CO as they give an estimate of about 45.3 Gg extrapolated for 2014. The slope corresponding to the evening rush hours (19:00 - 21:00) gives the highest estimate of CO. Using combinations of slopes for other periods also, the derived CO emissions are larger than the bottom-up EDGAR emission inventory. The EDGAR inventory estimates the relative contributions of CO from the industrial, transport and slum/residential sectors to be about 42, 42 and 10 % respectively. The possible cause for underestimation of CO by the EDGAR inventory could be the underestimation of residential emissions, since other inventories, particularly for major urban Indian cities (http://www.indiaenvironmentportal.org.in/files/file/Air-Pollution-in-Six-Indian-Cities.pdf), show large relative contributions from the residential sector. The uncertainty associated with the emission factors for different sectors could be another cause for the underestimation of CO emissions, since these are important parameters for developing the inventory (Sahu et al., 2015).

Table 2. Emission ratios of CO / CO$_2$ (ppb ppm^{-1}), derived from emission factors (gram of gases emitted per kilogram of fuel burned).

Biomass burning	Transport		Industry	Domestic	
Crop-residue[a,b,c]	Diesel[d,e,f]	Gasoline[d,f]	Coal	Coal[d,f]	Biofuel[c,d]
45.7–123.6	8.6–65.2	33.5	23.5–40.4	53.3–62.2	52.9–98.5

[a] Dhammapala et al. (2007); [b] Cao et al. (2008); [c] Andreae and Merlet (2001); [d] Streets et al. (2003);
[e] Sánchez-Ccoyllo et al. (2009); [f] Westerdahl et al. (2009)

Table 3. Estimates of emissions of CO using CO$_2$ emissions from the EDGAR inventory over the box (72.3 < longitude < 72.7° E, 22.8 < latitude < 23.2° N) and observed CO$_{(exc)}$: CO$_{2(exc)}$ slopes for different time periods. The correlation coefficient for corresponding slopes are given inside the brackets in the slope column. Data for the summer monsoon season are not included for calculating slopes.

| Time (IST)	Slope (ppb ppm^{-1}) Correlation coefficient (r)	EDGAR emissions (Gg year^{-2})		Estimated emissions (Gg year^{-2})
		CO$_2$	CO	
23:00–05:00	13 ± 0.14 (0.84)			69.2 ± 0.7
19:00–21:00	47 ± 0.27 0.95	8368.6	45.3	250.2 ± 1.5

5.1 Diurnal tracking of CO$_2$ emissions

CO has virtually no natural source in an urban environments except for oxidation of hydrocarbons and hence can help to disentangle the relative contributions of anthropogenic (from transport, power plant, industrial etc.) and biospheric (mainly from respiration) sources of CO$_2$, by serving as a tracer of combustion activity on a shorter timescale (Duren and Miller, 2012). Several studies have used simultaneously measured concentrations of CO$_2$ and CO to segregate the contributions of anthropogenic and natural biospheric sources in the total atmospheric concentrations of CO$_2$. The observed results are extensively validated using the carbon isotope (14CO$_2$) method. (Levin et al., 2003; Turnbull et al., 2006, 2011; Lopez et al., 2013; Newman et al., 2013). This quantification technique is more practical, less expensive and less time consuming in comparison to the ^{14}CO$_2$ method (Vogel et al., 2010). For performing this analysis, the background concentrations of CO and CO$_2$ and the emission ratio of CO/CO$_2$ from anthropogenic emissions are required. The methods for calculating the background concentrations of CO$_2$ and CO are already discussed in Sect. 4.4. The observed concentrations of these gases can also be directly used for calculating the emission ratio, provided that the measured levels are not highly affected by natural sources as well as sharing the same origin. We have used the evening time (19:00–21:00) data of CO$_{2(exc)}$ and CO$_{(exc)}$ for the whole study period to calculate the emission ratio of CO / CO$_2$ from the predominantly anthropogenic emission sources. The emission ratio for this time is calculated to be 47 ± 0.27 ppb ppm^{-1} with very high correlation ($r = 0.95$) (Fig. 8b), after excluding those data points for which the mean wind speed is greater than 3 ms^{-1}

in order to avoid the effect of fast ventilation. The tight correlations imply that there is not a substantial difference in the emission ratio of these gases during the measurement period from November 2013 to May 2015. CO$_{2(exc)}$ and CO$_{(exc)}$ will be poorly correlated with each other if their emission ratio varies largely with time, assuming the correlation is mainly driven by emissions. Since anthropogenic emissions are very high for this period, a contribution of respiration sources to the levels of CO$_2$ can be considered negligible during this period. This ratio can be considered to be representative of anthropogenic sources, as discussed in the previous section. We define it as $R_{CO / CO_{2(ant)}}$. The standard deviation shows the uncertainty associated with the slope, which is very small. The contribution of the transport sector (CO$_{2(ant)}$) to the diurnal cycle of CO$_2$ is calculated using the following formula.

$$CO_{(Ant)} = \frac{CO_{obs} - CO_{bg}}{R_{CO / CO_{2(ant)}}}, \qquad (2)$$

where CO$_{(obs)}$ is the observed CO concentration and CO$_{(bg)}$ is a background CO value. Uncertainty in the CO$_{2(ant)}$ is dominated by the uncertainty in the $R_{CO / CO_{2(ant)}}$ and by the choice of CO$_{(bg)}$. The uncertainty in CO$_{2(ant)}$ due to the uncertainty in the $R_{CO / CO_{2(ant)}}$ is about 0.5 % or 0.27 ppm and can be considered negligible. As discussed in Sect. 3, the uncertainty in the measurements of CO$_{(bg)}$ is very small and can also be considered negligible. Further, the contributions of CO$_2$ from the other major sources are calculated by subtracting the CO$_{2(ant)}$ from the excess concentrations of CO$_2$. These sources are those which do not emit significant amounts of CO and can be mostly considered as natural sources (respiration), denoted by CO$_{2(bio)}$.
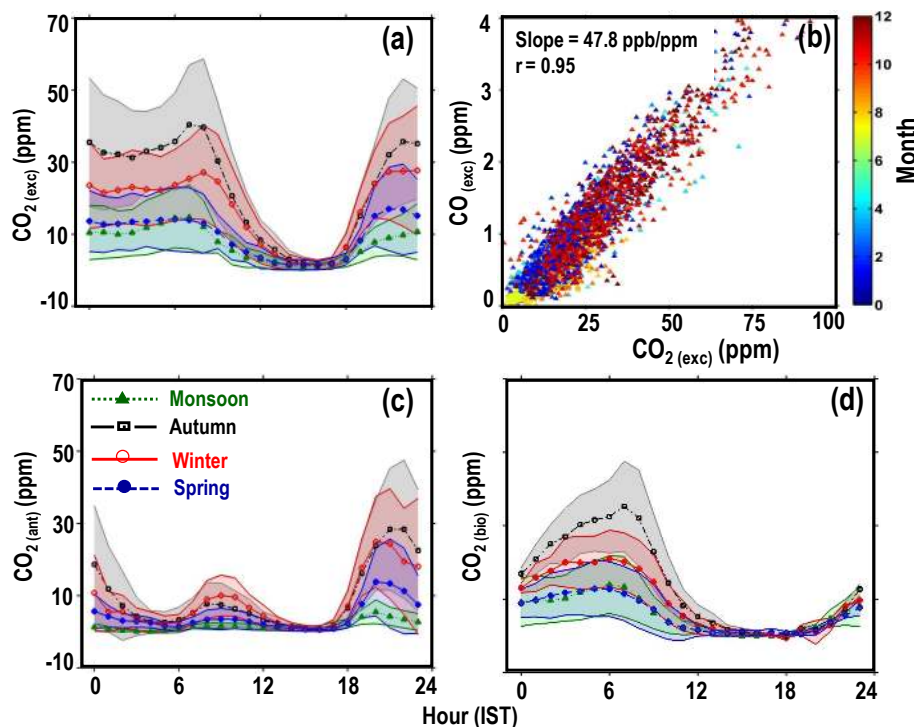
Figure 8. (a) Diurnal cycle of excess CO$_2$ over background levels during all four seasons. **(b)** Correlation between excess CO and CO$_2$ for evening hours (18:00–21:00) during the study period. Contributions of fossil fuel **(c)** and biosphere **(d)** in the diurnal variation of excess CO$_2$ in all four seasons.

The average diurnal cycles of CO$_2$ above the background for each season are shown in Fig. 8a. In Sect. 4.3.1, we have discussed qualitatively the role of different sources in the diurnal cycle of CO$_2$. With the help of the above method, the contributions of anthropogenic (CO$_{2(ant)}$) and biospheric sources (CO$_{2(bio)}$) are now discussed quantitatively. Due to the unavailability of PBL measurements, we cannot disentangle the contributions of boundary layer dynamics. The diurnal pattern of CO$_{2(ant)}$ (Fig. 8c) reflects the pattern of CO because we are using constant $R_{CO/CO_{2}(ant)}$ for all seasons. Overall, this analysis suggests that the anthropogenic emissions of CO$_2$, mostly from transport and industrial sectors during early morning between 06:00 and 10:00, varied from 15 to 60 % (4–15 ppm). During afternoon hours (11:00–17:00), the anthropogenic-originating (transport and industrial sources, mainly) CO$_2$ varied between 20 and 70 % (1–11 ppm). During evening rush hours (18:00–22:00), the highest contributions of combined emissions of anthropogenic sources (mainly transport and domestic) are observed. During this period the contributions vary from 50 to 95 % (2–44 ppm. During night/early morning hours (00:00–07:00) non-anthropogenic sources (mostly biospheric respiration) contribute from 8 to 41 ppm of CO$_2$ (Fig. 8d). The highest contributions from 18 to 41 ppm are observed in the autumn from the respiration sources during night hours, since there is more biomass after the southern Asian summer monsoon.

During the afternoon hours, the lower biospheric component of CO$_2$ could be due to a combination of the effects of afternoon anthropogenic emissions, biospheric uptake of CO$_2$ and higher PBL height.

5.2 Comparison of the model and observations

5.2.1 Comparison of diurnal cycle of CO$_2$

We first evaluate the ACTM in simulating the mean diurnal cycle of CO$_2$ over Ahmedabad by comparing the model-simulated surface-layer mean diurnal cycle of CO$_2$. The atmospheric concentrations of CO$_2$ are calculated by adding the anthropogenic, oceanic and biospheric component from the CASA process model. Figure 9a and b show the residuals (Hourly mean minus daily mean) of diurnal cycles of CO$_2$ based on the observations and the model simulations respectively. The model shows very little diurnal amplitude compared to the observations. Larger differences and discrepancies in night-time and morning CO$_2$ concentrations between the model and observations might be contributed to by diurnal cycles of the anthropogenic fluxes from local emissions and biospheric fluxes as well as by uncertainties in the estimation of PBL height by the model (Law et al., 2008). Hence, there is a need for efforts in improving the regional anthropogenic emissions as well as a module for estimating the PBL height. It may be pointed out that the model's horizon-
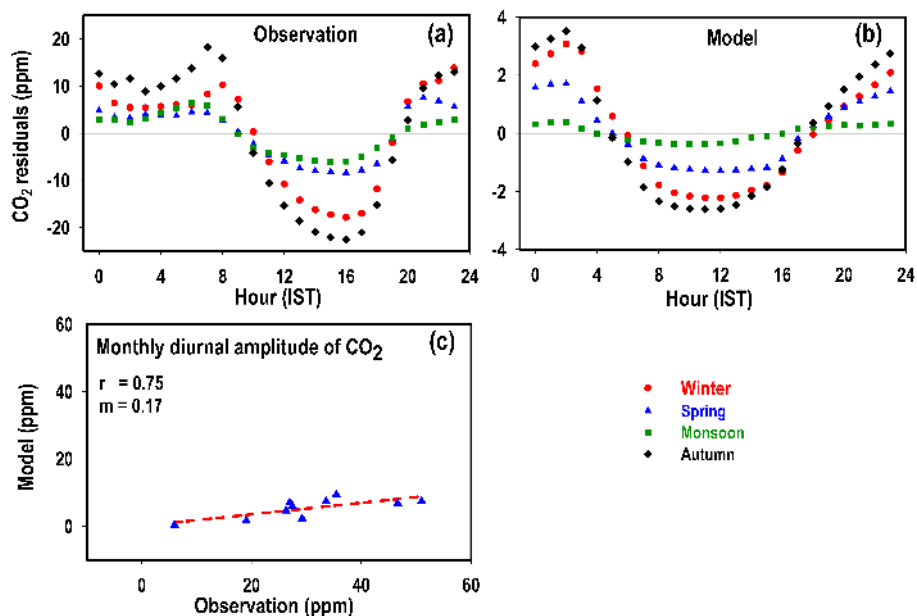
Figure 9. Residual of the diurnal cycle of CO$_2$ (in ppm) for **(a)** observations and **(b)** model simulation over Ahmedabad in all four seasons. Please note that the scales of the model and observational diurnal cycles are different. **(c)** Correlation between observed and the model simulated monthly mean diurnal cycle amplitudes.

tal resolution (1.125° × 1.125°) is too coarse for analysing local-scale observations. However, the model is able to capture the trend of the diurnal amplitude, highest in autumn and lowest in the summer monsoon season. Figure 9c shows better agreement ($r = 0.75$) between the monthly change in modelled and observational diurnal amplitude of CO$_2$ from monthly mean diurnal cycle however slope ($m = 0.17$) is very poor. We include the diurnal amplitudes of CO$_2$ for November and December 2013 also for improving the total number of data points. The model captured the spread in the daytime concentration of CO$_2$ from summer to spring with a difference that the model shows a lower concentration of CO$_2$ during noon hours in autumn while observations show the lowest concentration in the summer monsoon season.

The monthly average diurnal cycles of the biospheric net primary productivity from the CASA model for Ahmedabad and for the year 2014 are shown Fig. 10. The details of CASA flux are given in the Sect. 3.2. It is clear from Fig. 10 that the CO$_2$ flux diurnal cycle as modelled by CASA show minimum day-night variations amplitude during the summer monsoon time (June-July-August). Given that biosphere over Ahmedabad is water stressed for all other three seasons (except the summer monsoon time, Fig. 1A3), the behaviour of CASA model simulated diurnal variation is not in line with biological capacity of the plants to assimilate atmospheric CO$_2$. Due to this underestimation of CO$_2$ uptake in the summer monsoon season, we also find very large underestimation of the seasonal through by ACTM in comparison with observations (Fig. 9). Hence, there is a discrepancy in the diurnal flux of CO$_2$ simulated by CASA model. Similar discrepancy

Table 4. Performance matrices used to quantify the level of agreement between the model simulations and observations. These statistics are based on hourly values for each day.

| Parameter	Winter	Autumn	Summer	All months
MB (ppm)	−2.72	12.64	−2.45	2.27
FGE (%)	0.96	3.12	2.0	1.76
RMSE (ppm)	5.21	12.82	9.14	8.60
RMSE (%)	1.27	3.21	2.20	2.09

in the timing of maximum biospheric uptake is also discussed earlier by Patra et al. (2011) using inverse model CO$_2$ fluxes and CASA biospheric fluxes. It clearly suggests that there is a need for improving the biospheric flux for this region. It should be mentioned here that the CASA model used a land-use map from the late 1980s and early 1990s, which should be replaced by rapid growth in urbanized area in Ahmedabad (area and population increased by 91 and 42 % respectively, between 1990 and 2011). The model resolutions may be another factor for discrepancy. As Ballav et al. (2012) show that a regional model WRF-CO$_2$ is able to capture both diurnal and synoptic variations at two closely spaced stations within 25 km. Hence the regional models could be helpful for capturing these variabilities.

5.2.2 Comparison of seasonal cycle of CO$_2$

Figure 11a shows the performance of an ACTM-simulating mean seasonal cycle of CO$_2$ over Ahmedabad by compar-
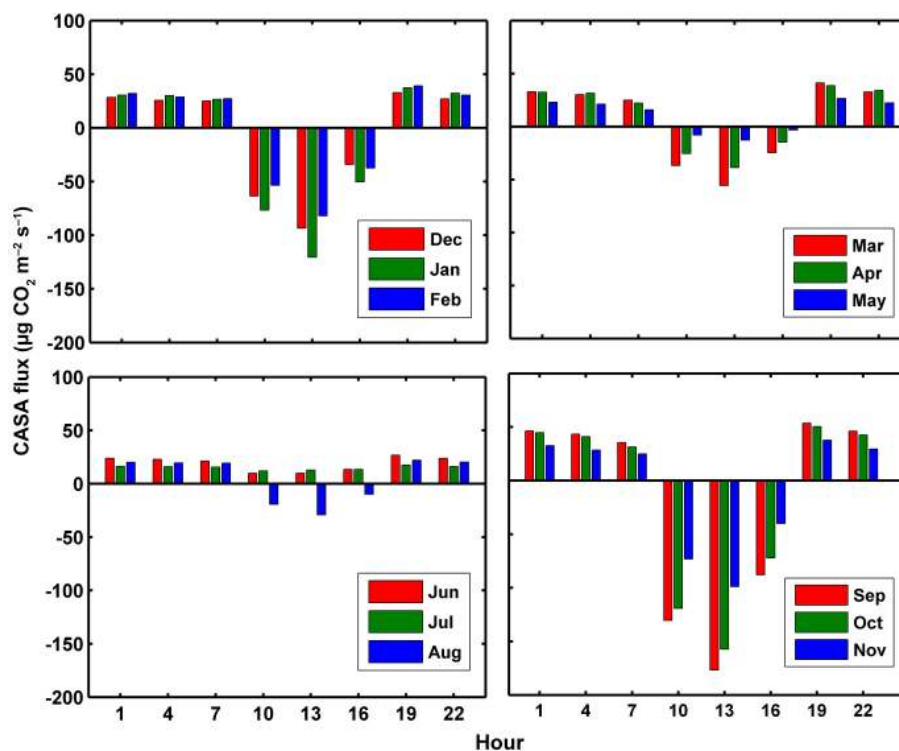
Figure 10. Diurnal variation of biospheric fluxes from the CASA ecosystem model.
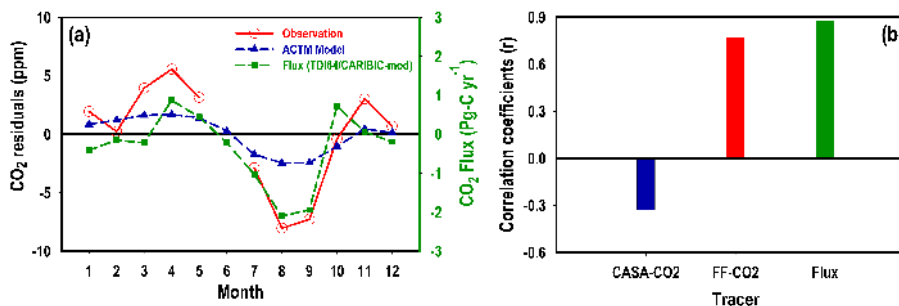
Figure 11. (a) The red circles and blue triangles show the mean seasonal cycles of CO$_2$ (in ppm) using afternoon values only, calculated from measurements over Ahmedabad and the model. The green triangles show the seasonal cycles of CO$_2$ flux over southern Asia, calculated from TDI64/CARIBIC-modified inverse model as given in Patra et al. (2011) (Fig. 3d). **(b)** Blue bar and red bar show the correlation coefficient (r) of model CO$_2$ concentration of biospheric tracer and fossil fuel tracer component with observed concentrations of CO$_2$, taking the entire annual time series of daily mean data. The green bar shows the correlation coefficient between the monthly residuals of afternoon mean only and the CO$_2$ flux over southern Asia.

ing it to the model-simulated mean surface seasonal cycle of CO$_2$. Due to the unavailability of data from March to June 2014, we plotted the monthly averages of the year 2015 for the same periods to visualize the complete seasonal cycle of CO$_2$. The seasonal cycles are calculated after subtracting the annual mean from each month and are corrected for growth rate using the observations at MLO. For comparison, we used the seasonal cycle calculated from afternoon average monthly concentrations, since the model is not able to capture the local fluctuations and produce better agree-

ments when boundary layer is well mixed. In Table 4 we present the summary of the comparisons of the model and observations. The model reproduces the observed seasonal cycle in CO$_2$ fairly well but with low seasonal amplitude at about 4.15 ppm compared to the 13.6 ppm observed. Positive bias during the summer monsoon season depicts the underestimation of biospheric productivity by the CASA model. The root mean square error is observed to be 3.21 % at its highest in the summer monsoon season. To understand the role of the biosphere, we also compared the seasonal cy-

Table 5. Seasonal mean concentrations and diurnal amplitudes (max–min) of CO$_2$ and CO over Ahmedabad.

Period	Mean (ppm)		Diurnal amplitude (ppm)	
	CO$_2$	CO	CO$_2$	CO
Monsoon	400.3 ± 6.8	0.19 ± 0.13	12.4	0.24
Autumn	419.6 ± 22.8	0.72 ± 0.71	40.9	1.36
Winter	417.2 ± 18.5	0.73 ± 0.68	31.7	1.01
Spring	415.4 ± 14.8	0.41 ± 0.40	15.9	0.62
Annual	413.0 ± 13.7	0.50 ± 0.37	25.0	0.48

cle of CO$_2$ from noontime mean data with the seasonal cycle of CO$_2$ fluxes over the southern Asian region, which is taken from Patra et al. (2011), where they calculated it using a inverse model with CARIBIC data and shifted a sink of 1.5 Pg C year^{-1} from July to August and termed it "TDI64/CARIBIC-modified". Positive and negative values of flux show the net release and net sink by the land biosphere over southern Asia. This comparison shows an almost one-to-one correlation in the monthly variation of CO$_2$ and suggests that the lower levels of CO$_2$ during July and August and the higher levels in April are mostly due to the moderate source and sink of the southern Asian ecosystem during these months. Significant correlation ($r = 0.88$) between southern Asian CO$_2$ fluxes and monthly mean CO$_2$ data for the daytime only suggest that the daytime levels of CO$_2$ are mostly controlled by the seasonal cycle of biosphere (Fig. 11b).

Separate correlations of each CO$_2$ tracer with the observations are helpful for determining the relative importance of each flux component in the CO$_2$ variation (Patra et al., 2008). Hence, we perform a separate correlation study between the measurements and biospheric, anthropogenic and oceanic components of CO$_2$, estimated by the model using CASA 3 h fluxes (Randerson et al., 1997; Olsen and Randerson, 2004), EDGAR v4.2 inventory and air–sea fluxes from Takahashi et al. (2009) respectively. The correlation coefficient indicates dominating controlling factors for deriving the levels of CO$_2$. Figure 11b shows the resulting correlations for a separate flux component with respect to measurements. We did not include the oceanic tracer and observed CO$_2$ correlation results, since no correlation has been observed between them. The comparison is based on the daily mean of the entire time series. The correlation between biospheric tracers and observed CO$_2$ has been found to be negative. This is because during the growing season, biospheric sources act as a net sink for CO$_2$. A correlation of observed CO$_2$ with the fossil fuel tracer has been identified fairly well ($r = 0.75$). Hence, a correlation study of individual tracers also gives evidence of the overall dominance of fossil flux in overall concentrations of CO$_2$ over Ahmedabad for the entire study period and by assuming fossil fuel CO$_2$ emissions we can derive meaningful information on the biospheric uptake cycle.

This study suggests that the model is able to capture seasonal cycles at lower amplitude for Ahmedabad. However, the model fails to capture the diurnal variability since local transport and hourly daily flux play important roles for governing the diurnal cycle and hence there is a need for improving these features of the model.

6 Conclusions

Atmospheric concentrations of CO$_2$ were measured along with an anthropogenic tracer CO at Ahmedabad, a semi-arid urban region in western India, using a laser-based CRDS technique during 2013–2015. The air masses, originating from both polluted continental and cleaner marine regions over the study location during different seasons, make this study most important for studying the characteristics of both types of air masses. The observations show a large range of variability in CO$_2$ concentrations (from 382 to 609 ppm) and CO concentrations (from 0.07 to 8.8 ppm), with averages of 416 ± 19 ppm and 0.61 ± 0.6 ppm respectively. Higher concentrations of the gases are recorded for lower ventilation and winds from a north-easterly direction, while the lowest concentrations are observed for higher ventilation and the cleaner south-westerly winds from the Indian Ocean. Along with these factors, the biospheric activity also controls the seasonal cycle of CO$_2$. The lowest daytime CO$_2$ concentrations, ranging from 382 to 393 ppm in August, suggest a stronger biospheric productivity during this month over the study region in agreement with an earlier inverse modelling study. This is in contrast to the terrestrial flux simulated by the CASA ecosystem model, showing highest productivity in September and October. Hence, the seasonal cycles of the gases reflect the seasonal variations of natural sources and sinks, anthropogenic emissions and seasonally varying atmospheric transport. The annual amplitudes of CO$_2$ variation after subtracting the growth rate based on the Mauna Loa, Hawaii data are observed to be about 26.07 ppm using the monthly mean of all data and 13.6 ppm using the monthly mean of the afternoon (12:00–16:00) data only. Significant differences between these amplitudes suggests that the annual amplitude from the afternoon monthly mean data only does not give a true picture of the variability. It is to be noted that most of the CO$_2$ measurements in India are based on daytime flask samplings only.

Significant differences in the diurnal patterns of CO$_2$ and CO are also observed, even though both gases have major common emission sources and undergo PBL dynamics and advection. Differences in their diurnal variability are probably the effect of the terrestrial biosphere on CO$_2$ and chemical loss of CO due to reaction with OH radicals. The morning and evening peaks of CO are affected by rush hour traffic and PBL height variability, and they occur at almost the same time throughout the year. However, the morning peaks in CO$_2$ change their time slightly due to a shift in photo-

synthesis activity according to change in sunrise time during different seasons. The amplitudes of annual average diurnal cycles of CO$_2$ and CO are observed at about 25 and 0.48 ppm respectively (Table 5). Both gases show highest amplitude in the autumn and lowest in the summer monsoon season. This shows that major influencing processes are common for the gases, specific to the city and the Indian monsoon.

The availability of simultaneous and continuous measurements of CO$_2$ and CO have made it possible to study their correlations at different time windows (during morning (06:00–10:00), noon (11:00–17:00), evening (18:00–22:00) and night (00:00–05:00) hours) of distinct seasons. Using the correlation slopes and comparing them with the emission ratios of different sources, contributions of distinct sources are discussed qualitatively. It is observed that during the evening hours, measurements over the study region are mostly affected by transport and domestic sources, while during other periods the levels of both gases are mostly dominated by emissions from transport and industrial sources. Further, using the slope from the evening rush hour (18:00–22:00) data as anthropogenic emission ratios, the relative contributions of dominant anthropogenic emissions and biospheric emissions have been disentangled from the diurnal cycle of CO$_2$. At rush hour, this analysis suggests that 90–95 % of the total emissions of CO$_2$ are contributed by anthropogenic emissions. The total yearly emission of CO for Ahmedabad has also been estimated using these measurements. In this estimation, fossil-fuel-derived emissions of CO$_2$ from the EDGAR v4.2 inventory are extrapolated linearly from 2008 to 2014 and it is assumed that there are no year-to-year variations in the land biotic and oceanic CO$_2$ emissions. The estimated annual CO emission for Ahmedabad is estimated to be 69.2 ± 0.7 Gg for the year 2014. The extrapolated CO emission from the EDGAR inventory for 2014 shows a value smaller than this estimate by about 52 %.

The observed results of CO$_2$ are also compared with a general atmospheric circulation model based on chemistry-transport model-simulated CO$_2$ concentrations. The model captures some basic features like the trend of diurnal amplitude, seasonal amplitude etc. qualitatively but not quantitatively. The model captures the seasonal cycle fairly well but the amplitude is much lower compared to the observations. Similarly, performance of the model capturing the change in monthly averaged diurnal amplitude is quite good ($r = 0.72$), however the slope is very poor. We also examined the correlation between the hourly averaged observed CO$_2$ and tracer of fossil fuel from model simulation and found fairly good correlation between them. However, no significant correlation has been observed between observed CO$_2$ and biospheric tracer. It suggests that the levels of CO$_2$ over Ahmedabad are mostly controlled by fossil fuel combustion throughout the year.

This work demonstrates the usefulness of simultaneous measurements of CO$_2$ and CO in an urban region. The anthropogenic and biospheric components of CO$_2$ have been studied from its temporally varying atmospheric concentrations, and validity of the "bottom-up" inventory has been assessed independently. Use of CO$_{(exc)}$: CO$_{2(exc)}$ ratios avoids some of the problems with assumptions that have to be made with modelling. These results represent a major urban region of India and will be helpful in validating emission inventories, chemistry-transport and terrestrial ecosystem models. However, a bigger network of sites is needed to elucidate more accurate distributions of emissions and their source regions and run continuously over multiple years for tracking the changes associated with anthropogenic activities and emission mitigation policies. The corresponding author may be contacted for the data published in this article.

References

Ahmadov, R., Gerbig, C., Kretschmer, R., Koerner, S., Neininger, B., Dolman, A. J., and Sarrat, C.: Mesoscale covariance of transport and CO$_2$ fluxes: Evidence from observations and simulations using the WRF-VPRM coupled atmosphere-biosphere model, J. Geophys. Res.-Atmos., 112, D22107, doi:10.1029/2007JD008552, 2007.

Ammoura, L., Xueref-Remy, I., Gros, V., Baudic, A., Bonsang, B., Petit, J.-E., Perrussel, O., Bonnaire, N., Sciare, J., and Chevallier, F.: Atmospheric measurements of ratios between CO$_2$ and co-emitted species from traffic: a tunnel study in the Paris megacity, Atmos. Chem. Phys., 14, 12871–12882, doi:10.5194/acp-14-12871-2014, 2014.

Andreae, M. O. and Merlet, P.: Emission of trace gases and aerosols from biomass burning, Global Biogeochem. Cy., 15, 955–966, doi:10.1029/2000GB001382, 2001.

Baker, A. K., Schuck, T. J., Brenninkmeijer, C. A. M., Rauthe-Schöch, A., Slemr, F., van Velthoven, P. F. J., and Lelieveld, J.: Estimating the contribution of monsoon-related biogenic production to methane emissions from South Asia using CARIBIC observations, Geophys. Res. Lett., 39, l10813, doi:10.1029/2012GL051756, 2012.

Ballav, S., Patra, P. K., Takigawa, M., Ghosh, S., De, U. K., Maksyutov, S., Murayama, S., Mukai, H., and Hashimoto, S.: Simulation of CO$_2$ Concentration over East Asia Using the Regional Transport Model WRF-CO2, J. Meteorol. Soc. Jpn., 90, 959–976, doi:10.2151/jmsj.2012-607, 2012.

Ballav, S., Patra, P. K., Sawa, Y., Matsueda, H., Adachi, A., Onogi, S., Takigawa, M., and De, U.: Simulation of CO$_2$ concentrations at Tsukuba tall tower using WRF−CO$_2$ tracer transport model, J. Earth Syst. Sci., 125, 47–64, doi:10.1007/s12040-015-0653-y, 2015.

Bhattacharya, S. K., Borole, D. V., Francey, R. J., Allison, C. E., Steele, L. P., Krummel, P., Langenfelds, R., Masarie, K. A., Tiwari, Y. K., and Patra, P.: Trace gases and CO$_2$ isotope records from Cabo de Rama, India, Curr. Sci., 97, 1336–1344, 2009.

Bitter, M., Ball, S. M., Povey, I. M., and Jones, R. L.: A broadband cavity ringdown spectrometer for in-situ measurements of atmospheric trace gases, Atmos. Chem. Phys., 5, 2547–2560, doi:10.5194/acp-5-2547-2005, 2005.

Brenninkmeijer, C. A. M., Crutzen, P., Boumard, F., Dauer, T., Dix, B., Ebinghaus, R., Filippi, D., Fischer, H., Franke, H., Frieß, U., Heintzenberg, J., Helleis, F., Hermann, M., Kock, H. H., Koeppel, C., Lelieveld, J., Leuenberger, M., Martinsson, B. G., Miemczyk, S., Moret, H. P., Nguyen, H. N., Nyfeler, P., Oram, D., O'Sullivan, D., Penkett, S., Platt, U., Pupek, M., Ramonet, M., Randa, B., Reichelt, M., Rhee, T. S., Rohwer, J., Rosenfeld, K., Scharffe, D., Schlager, H., Schumann, U., Slemr, F., Sprung, D., Stock, P., Thaler, R., Valentino, F., van Velthoven, P., Waibel, A., Wandel, A., Waschitschek, K., Wiedensohler, A., Xueref-Remy, I., Zahn, A., Zech, U., and Ziereis, H.: Civil Aircraft for the regular investigation of the atmosphere based on an instrumented container: The new CARIBIC system, Atmos. Chem. Phys., 7, 4953–4976, doi:10.5194/acp-7-4953-2007, 2007.

Briber, B. M., Hutyra, L. R., Dunn, A. L., Raciti, S. M., and Munger, J. W.: Variations in Atmospheric CO$_2$ Mixing Ratios across a Boston, MA Urban to Rural Gradient, Land, 2, 304, doi:10.3390/land2030304, 2013.

Cao, G., Zhang, X., Gong, S., and Zheng, F.: Investigation on emission factors of particulate matter and gaseous pollutants from crop residue burning, J. Environ. Sci., 20, 50–55, doi:10.1016/S1001-0742(08)60007-8, 2008.

Chen, H., Winderlich, J., Gerbig, C., Hoefer, A., Rella, C. W., Crosson, E. R., Van Pelt, A. D., Steinbach, J., Kolle, O., Beck, V., Daube, B. C., Gottlieb, E. W., Chow, V. Y., Santoni, G. W., and Wofsy, S. C.: High-accuracy continuous airborne measurements of greenhouse gases (CO$_2$ and CH$_4$) using the cavity ring-down spectroscopy (CRDS) technique, Atmos. Meas. Tech., 3, 375–386, doi:10.5194/amt-3-375-2010, 2010.

Ciais, P., Sabine, C., Bala, G., Bopp, L., Brovkin, V., Canadell, J., Chhabra, A., DeFries, R., Galloway, J., Heimann, M., Jones, C., Quere, C., Myneni, R., Piao, S., and Thornton, P.: Carbon and Other Biogeochemical Cycles, book section 6, Cambridge University Press, Cambridge, United Kingdom and New York, NY, USA, 465–570, doi:10.1017/CBO9781107415324.015, 2013.

Crosson, E.: A cavity ring-down analyzer for measuring atmospheric levels of methane, carbon dioxide, and water vapor, Appl. Phys. B, 92, 403–408, doi:10.1007/s00340-008-3135-y, 2008.

Dhammapala, R., Claiborn, C., Simpson, C., and Jimenez, J.: Emission factors from wheat and Kentucky bluegrass stubble burning: Comparison of field and simulated burn experiments, Atmos. Environ., 41, 1512–1520, doi:10.1016/j.atmosenv.2006.10.008, 2007.

Duren, R. M. and Miller, C. E.: Measuring the carbon emissions of megacities, Nature Clim. Change, 2, 560–562, doi:10.1038/nclimate1629, 2012.

EDGAR Project Team:, Emission Database for Global Atmospheric Research (EDGAR), release version 4.2., doi:10.2904/EDGARv4.2, http://edgar.jrc.ec.europa.eu, 2011.

Kar, J., Bremer, H., Drummond, J. R., Rochon, Y. J., Jones, D. B. A., Nichitiu, F., Zou, J., Liu, J., Gille, J. C., Edwards, D. P., Deeter, M. N., Francis, G., Ziskin, D., and Warner, J.: Evidence of vertical transport of carbon monoxide from Measurements of Pollution in the Troposphere (MOPITT), Geophys. Res. Lett., 31, L23105, doi:10.1029/2004GL021128, 2004.

Karion, A., Sweeney, C., Wolter, S., Newberger, T., Chen, H., Andrews, A., Kofler, J., Neff, D., and Tans, P.: Long-term greenhouse gas measurements from aircraft, Atmos. Meas. Tech., 6, 511–526, doi:10.5194/amt-6-511-2013, 2013.

Lai, S. C., Baker, A. K., Schuck, T. J., van Velthoven, P., Oram, D. E., Zahn, A., Hermann, M., Weigelt, A., Slemr, F., Brenninkmeijer, C. A. M., and Ziereis, H.: Pollution events observed during CARIBIC flights in the upper troposphere between South China and the Philippines, Atmos. Chem. Phys., 10, 1649–1660, doi:10.5194/acp-10-1649-2010, 2010.

Lal, S., Naja, M., and Subbaraya, B.: Seasonal variations in surface ozone and its precursors over an urban site in India, Atmos. Environ., 34, 2713–2724, doi:10.1016/S1352-2310(99)00510-5, 2000.

Lal, S., Chandra, N., and Venkataramani, S.: A study of CO$_2$ and related trace gases using a laser based technique at an urban site in western India, Curr. Sci., 109, 2111–2116, 2015.

Law, R. M., Peters, W., Rödenbeck, C., Aulagnier, C., Baker, I., Bergmann, D. J., Bousquet, P., Brandt, J., Bruhwiler, L., Cameron-Smith, P. J., Christensen, J. H., Delage, F., Denning, A. S., Fan, S., Geels, C., Houweling, S., Imasu, R., Karstens, U., Kawa, S. R., Kleist, J., Krol, M. C., Lin, S.-J., Lokupitiya, R., Maki, T., Maksyutov, S., Niwa, Y., Onishi, R., Parazoo, N., Patra, P. K., Pieterse, G., Rivier, L., Satoh, M., Serrar, S., Taguchi, S., Takigawa, M., Vautard, R., Vermeulen, A. T., and Zhu, Z.: TransCom model simulations of hourly atmospheric CO$_2$: Experimental overview and diurnal cycle results for 2002, Global Biogeochem. Cy., 22, gB3009, doi:10.1029/2007GB003050, 2008.

Le Quéré, C., Moriarty, R., Andrew, R. M., Peters, G. P., Ciais, P., Friedlingstein, P., Jones, S. D., Sitch, S., Tans, P., Arneth, A., Boden, T. A., Bopp, L., Bozec, Y., Canadell, J. G., Chini, L. P., Chevallier, F., Cosca, C. E., Harris, I., Hoppema, M., Houghton, R. A., House, J. I., Jain, A. K., Johannessen, T., Kato, E., Keeling, R. F., Kitidis, V., Klein Goldewijk, K., Koven, C., Landa, C. S., Landschützer, P., Lenton, A., Lima, I. D., Marland, G., Mathis, J. T., Metzl, N., Nojiri, Y., Olsen, A., Ono, T., Peng, S., Peters, W., Pfeil, B., Poulter, B., Raupach, M. R., Regnier, P., Rödenbeck, C., Saito, S., Salisbury, J. E., Schuster, U., Schwinger, J., Séférian, R., Segschneider, J., Steinhoff, T., Stocker, B. D., Sutton, A. J., Takahashi, T., Tilbrook, B., van der Werf, G. R., Viovy, N., Wang, Y.-P., Wanninkhof, R., Wiltshire, A., and Zeng, N.: Global carbon budget 2014, Earth Syst. Sci. Data, 7, 47–85, doi:10.5194/essd-7-47-2015, 2015.

Levin, I., Kromer, B., Schmidt, M., and Sartorius, H.: A novel approach for independent budgeting of fossil fuel CO$_2$ over Europe by ^{14}CO$_2$ observations, Geophys. Res. Lett., 30, 2194, doi:10.1029/2003GL018477, 2003.

Lin, X., Indira, N. K., Ramonet, M., Delmotte, M., Ciais, P., Bhatt, B. C., Reddy, M. V., Angchuk, D., Balakrishnan, S., Jorphail, S.,

Dorjai, T., Mahey, T. T., Patnaik, S., Begum, M., Brenninkmeijer, C., Durairaj, S., Kirubagaran, R., Schmidt, M., Swathi, P. S., Vinithkumar, N. V., Yver Kwok, C., and Gaur, V. K.: Long-lived atmospheric trace gases measurements in flask samples from three stations in India, Atmos. Chem. Phys., 15, 9819–9849, doi:10.5194/acp-15-9819-2015, 2015.

Lopez, M., Schmidt, M., Delmotte, M., Colomb, A., Gros, V., Janssen, C., Lehman, S. J., Mondelain, D., Perrussel, O., Ramonet, M., Xueref-Remy, I., and Bousquet, P.: CO, NO$_x$ and ^{13}CO$_2$ as tracers for fossil fuel CO$_2$: results from a pilot study in Paris during winter 2010, Atmos. Chem. Phys., 13, 7343–7358, doi:10.5194/acp-13-7343-2013, 2013.

Machida, T., Matsueda, H., Sawa, Y., Nakagawa, Y., Hirotani, K., Kondo, N., Goto, K., Nakazawa, T., Ishikawa, K., and Ogawa, T.: Worldwide Measurements of Atmospheric CO$_2$ and Other Trace Gas Species Using Commercial Airlines, J. Atmos. Ocean. Tech., 25, 1744–1754, doi:10.1175/2008JTECHA1082.1, 2008.

Mahesh, P., Sharma, N., Dadhwal, V., Rao, P., Apparao, B., Ghosh, A., Mallikarjun, K., and Ali, M.: Impact of Land-Sea Breeze and Rainfall on CO$_2$ Variations at a Coastal Station, J. Earth Sci. Clim. Change, 5, 201, doi:10.4172/2157-7617.1000201, 2014.

Mallik, C., Lal, S., and Venkataramani, S.: Trace gases at a semi-arid urban site in western India: variability and inter-correlations, J. Atmos. Chem., 72, 243–264, doi:10.1007/s10874-015-9311-7, 2015.

Mallik, C., Chandra, N., Venkataramani, S., and Lal, S.: Variability of atmospheric carbonyl sulfide at a semi-arid urban site in western India, Sci. Total Environ., 551–552, 725–737, doi:10.1016/j.scitotenv.2016.02.014, 2016.

Newman, S., Jeong, S., Fischer, M. L., Xu, X., Haman, C. L., Lefer, B., Alvarez, S., Rappenglueck, B., Kort, E. A., Andrews, A. E., Peischl, J., Gurney, K. R., Miller, C. E., and Yung, Y. L.: Diurnal tracking of anthropogenic CO$_2$ emissions in the Los Angeles basin megacity during spring 2010, Atmos. Chem. Phys., 13, 4359–4372, doi:10.5194/acp-13-4359-2013, 2013.

Olsen, S. C. and Randerson, J. T.: Differences between surface and column atmospheric CO$_2$ and implications for carbon cycle research, J. Geophys. Res.-Atmos., 109, d02301, doi:10.1029/2003JD003968, 2004.

Onogi, K., Tsutsui, J., Koide, H., Sakamoto, M., Kobayashi, S., Hatsushika, H., Matsumoto, T., Yamazaki, N., Kamahori, H., Takahashi, K., Kadokura, S., Wada, K., Kato, K., Oyama, R., Ose, T., Mannoji, N., and Taira, R.: The JRA-25 Reanalysis, J. Meteorol. Soc. Jpn. Ser. II, 85, 369–432, doi:10.2151/jmsj.85.369, 2007.

Park, M., Randel, W. J., Emmons, L. K., and Livesey, N. J.: Transport pathways of carbon monoxide in the Asian summer monsoon diagnosed from Model of Ozone and Related Tracers (MOZART), J. Geophys. Res., 114, D08303, doi:10.1029/2008JD010621, 2009.

Patra, P. K., Law, R. M., Peters, W., Rödenbeck, C., Takigawa, M., Aulagnier, C., Baker, I., Bergmann, D. J., Bousquet, P., Brandt, J., Bruhwiler, L., Cameron-Smith, P. J., Christensen, J. H., Delage, F., Denning, A. S., Fan, S., Geels, C., Houweling, S., Imasu, R., Karstens, U., Kawa, S. R., Kleist, J., Krol, M. C., Lin, S.-J., Lokupitiya, R., Maki, T., Maksyutov, S., Niwa, Y., Onishi, R., Parazoo, N., Pieterse, G., Rivier, L., Satoh, M., Serrar, S., Taguchi, S., Vautard, R., Vermeulen, A. T., and Zhu, Z.: TransCom model simulations of hourly atmospheric CO$_2$: Analysis of synoptic-scale varia-

tions for the period 2002–2003, Global Biogeochem. Cy., 22, doi:10.1029/2007GB003081, gB4013, 2008.

Patra, P. K., Niwa, Y., Schuck, T. J., Brenninkmeijer, C. A. M., Machida, T., Matsueda, H., and Sawa, Y.: Carbon balance of South Asia constrained by passenger aircraft CO$_2$ measurements, Atmos. Chem. Phys., 11, 4163–4175, doi:10.5194/acp-11-4163-2011, 2011.

Patra, P. K., Canadell, J. G., Houghton, R. A., Piao, S. L., Oh, N.-H., Ciais, P., Manjunath, K. R., Chhabra, A., Wang, T., Bhattacharya, T., Bousquet, P., Hartman, J., Ito, A., Mayorga, E., Niwa, Y., Raymond, P. A., Sarma, V. V. S. S., and Lasco, R.: The carbon budget of South Asia, Biogeosciences, 10, 513–527, doi:10.5194/bg-10-513-2013, 2013.

Pérez-Landa, G., Ciais, P., Gangoiti, G., Palau, J. L., Carrara, A., Gioli, B., Miglietta, F., Schumacher, M., Millán, M. M., and Sanz, M. J.: Mesoscale circulations over complex terrain in the Valencia coastal region, Spain – Part 2: Modeling CO$_2$ transport using idealized surface fluxes, Atmos. Chem. Phys., 7, 1851–1868, doi:10.5194/acp-7-1851-2007, 2007.

Peylin, P., Law, R. M., Gurney, K. R., Chevallier, F., Jacobson, A. R., Maki, T., Niwa, Y., Patra, P. K., Peters, W., Rayner, P. J., Rödenbeck, C., van der Laan-Luijkx, I. T., and Zhang, X.: Global atmospheric carbon budget: results from an ensemble of atmospheric CO$_2$ inversions, Biogeosciences, 10, 6699–6720, doi:10.5194/bg-10-6699-2013, 2013.

Randel, W. J. and Park, M.: Deep convective influence on the Asian summer monsoon anticyclone and associated tracer variability observed with Atmospheric Infrared Sounder (AIRS), J. Geophys. Res., 111, D12314, doi:10.1029/2005JD006490, 2006.

Randerson, J. T., Thompson, M. V., Conway, T. J., Fung, I. Y., and Field, C. B.: The contribution of terrestrial sources and sinks to trends in the seasonal cycle of atmospheric carbon dioxide, Global Biogeochem. Cy., 11, 535–560, doi:10.1029/97GB02268, 1997.

Russo, R. S., Talbot, R. W., Dibb, J. E., Scheuer, E., Seid, G., Jordan, C. E., Fuelberg, H. E., Sachse, G. W., Avery, M. A., Vay, S. A., Blake, D. R., Blake, N. J., Atlas, E., Fried, A., Sandholm, S. T., Tan, D., Singh, H. B., Snow, J., and Heikes, B. G.: Chemical composition of Asian continental outflow over the western Pacific: Results from Transport and Chemical Evolution over the Pacific (TRACE-P), J. Geophys. Res., 108, 8804, doi:10.1029/2002JD003184, 2003.

Sahu, L. and Lal, S.: Distributions of C2–C5 {NMHCs} and related trace gases at a tropical urban site in India, Atmos. Environ., 40, 880–891, doi:10.1016/j.atmosenv.2005.10.021, 2006.

Sahu, S., Beig, G., and Parkhi, N.: High Resolution Emission Inventory of NOx and CO for Mega City Delhi, India, Aerosol Air Qual. Res., 15, 1137–1144, doi:10.4209/aaqr.2014.07.0132, 2015.

Sánchez-Ccoyllo, O., Ynoue, R., Martins, L., Astolfo, R., Miranda, R., Freitas, E., Borges, A., Fornaro, A., Freitas, H., Moreira, A., and Andrade, M.: Vehicular particulate matter emissions in road tunnels in Sao Paulo, Brazil, Environ. Monit. Assess., 149, 241–249, doi:10.1007/s10661-008-0198-5, 2009.

Schuck, T. J., Brenninkmeijer, C. A. M., Baker, A. K., Slemr, F., von Velthoven, P. F. J., and Zahn, A.: Greenhouse gas relationships in the Indian summer monsoon plume measured by the CARIBIC passenger aircraft, Atmos. Chem. Phys., 10, 3965–3984, doi:10.5194/acp-10-3965-2010, 2010.

Schuck, T. J., Ishijima, K., Patra, P. K., Baker, A. K., Machida, T., Matsueda, H., Sawa, Y., Umezawa, T., Brenninkmeijer, C. A. M., and Lelieveld, J.: Distribution of methane in the tropical upper troposphere measured by CARIBIC and CONTRAIL aircraft, J. Geophys. Res.-Atmos., 117, d19304, doi:10.1029/2012JD018199, 2012.

Sharma, N., Dadhwal, V., Kant, Y., Mahesh, P., Mallikarjun, K., Gadavi, H., Sharma, A., and Ali, M.: Atmospheric CO$_2$ Variations in Two Contrasting Environmental Sites Over India, Air Soil Water Res., 7, 61–68, doi:10.4137/ASWR.S13987, 2014.

Streets, D. G., Bond, T. C., Carmichael, G. R., Fernandes, S. D., Fu, Q., He, D., Klimont, Z., Nelson, S. M., Tsai, N. Y., Wang, M. Q., Woo, J.-H., and Yarber, K. F.: An inventory of gaseous and primary aerosol emissions in Asia in the year 2000, J. Geophys. Res., 108, 8809, doi:10.1029/2002JD003093, 2003.

Suntharalingam, P., Jacob, D. J., Palmer, P. I., Logan, J. A., Yantosca, R. M., Xiao, Y., Evans, M. J., Streets, D. G., Vay, S. L., and Sachse, G. W.: Improved quantification of Chinese carbon fluxes using CO$_2$/CO correlations in Asian outflow, J. Geophys. Res., 109, D18S18, doi:10.1029/2003JD004362, 2004.

Takahashi, T., Sutherland, S. C., Wanninkhof, R., Sweeney, C., Feely, R. A., Chipman, D. W., Hales, B., Friederich, G., Chavez, F., Sabine, C., Watson, A., Bakker, D. C., Schuster, U., Metzl, N., Yoshikawa-Inoue, H., Ishii, M., Midorikawa, T., Nojiri, Y., Körtzinger, A., Steinhoff, T., Hoppema, M., Olafsson, J., Arnarson, T. S., Tilbrook, B., Johannessen, T., Olsen, A., Bellerby, R., Wong, C., Delille, B., Bates, N., and de Baar, H. J.: Climatological mean and decadal change in surface ocean pCO2, and net sea–air {CO$_2$} flux over the global oceans, Deep Sea Research Part II: Topical Studies in Oceanography, 56, 554–577, doi:10.1016/j.dsr2.2008.12.009, 2009.

Takegawa, N., Kondo, Y., Koike, M., Chen, G., Machida, T., Watai, T., Blake, D. R., Streets, D. G., Woo, J.-H., Carmichael, G. R., Kita, K., Miyazaki, Y., Shirai, T., Liley, J. B., and Ogawa, T.: Removal of NOx and NOy in Asian outflow plumes: Aircraft measurements over the western Pacific in January 2002, J. Geophys. Res., 109, D23S04, doi:10.1029/2004JD004866, 2004.

Tiwari, Y. K., Vellore, R. K., Kumar, K. R., van der Schoot, M., and Cho, C.-H.: Influence of monsoons on atmospheric CO$_2$ spatial variability and ground-based monitoring over India, Sci. Total Environ., 490, 570–578, doi:10.1016/j.scitotenv.2014.05.045, 2014.

Turnbull, J. C., Miller, J. B., Lehman, S. J., Tans, P. P., Sparks, R. J., and Southon, J.: Comparison of 14CO$_2$, CO, and SF$_6$ as tracers for recently added fossil fuel CO$_2$ in the atmosphere and implications for biological CO$_2$ exchange, Geophys. Res. Lett., 33, L01817, doi:10.1029/2005GL024213, 2006.

Turnbull, J. C., Karion, A., Fischer, M. L., Faloona, I., Guilderson, T., Lehman, S. J., Miller, B. R., Miller, J. B., Montzka, S., Sherwood, T., Saripalli, S., Sweeney, C., and Tans, P. P.: Assessment of fossil fuel carbon dioxide and other anthropogenic trace gas emissions from airborne measurements over Sacramento, California in spring 2009, Atmos. Chem. Phys., 11, 705–721, doi:10.5194/acp-11-705-2011, 2011.

Vogel, F. R., Hammer, S., Steinhof, A., Kromer, B., and Levin, I.: Implication of weekly and diurnal 14C calibration on hourly estimates of CO-based fossil fuel CO$_2$ at a moderately polluted site in southwestern Germany, Tellus B, 62, 512–520, doi:10.1111/j.1600-0889.2010.00477.x, 2010.

Wada, A., Matsueda, H., Sawa, Y., Tsuboi, K., and Okubo, S.: Seasonal variation of enhancement ratios of trace gases observed over 10 years in the western North Pacific, Atmos. Environ., 45, 2129–2137, doi:10.1016/j.atmosenv.2011.01.043, 2011.

Wang, Y., Munger, J. W., Xu, S., McElroy, M. B., Hao, J., Nielsen, C. P., and Ma, H.: CO$_2$ and its correlation with CO at a rural site near Beijing: implications for combustion efficiency in China, Atmos. Chem. Phys., 10, 8881–8897, doi:10.5194/acp-10-8881-2010, 2010.

Welp, L. R., Keeling, R. F., Weiss, R. F., Paplawsky, W., and Heckman, S.: Design and performance of a Nafion dryer for continuous operation at CO$_2$ and CH$_4$ air monitoring sites, Atmos. Meas. Tech., 6, 1217–1226, doi:10.5194/amt-6-1217-2013, 2013.

Westerdahl, D., Wang, X., Pan, X., and Zhang, K. M.: Characterization of on-road vehicle emission factors and microenvironmental air quality in Beijing, China, Atmos. Environ., 43, 697–705, doi:10.1016/j.atmosenv.2008.09.042, 2009.

Wong, K. W., Fu, D., Pongetti, T. J., Newman, S., Kort, E. A., Duren, R., Hsu, Y.-K., Miller, C. E., Yung, Y. L., and Sander, S. P.: Mapping CH$_4$: CO$_2$ ratios in Los Angeles with CLARS-FTS from Mount Wilson, California, Atmos. Chem. Phys., 15, 241–252, doi:10.5194/acp-15-241-2015, 2015.

Wunch, D., Wennberg, P. O., Toon, G. C., Keppel-Aleks, G., and Yavin, Y. G.: Emissions of greenhouse gases from a North American megacity, Geophys. Res. Lett., 36, L15810, doi:10.1029/2009GL039825, 2009.